CHALMERS
UNIVERSITY OF TECHNOLOGY

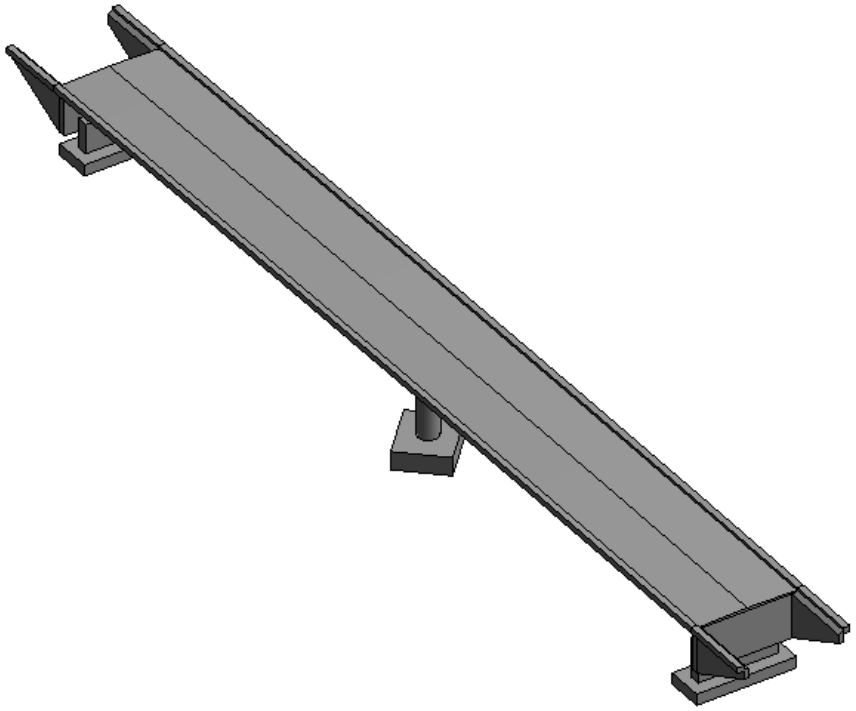

Early Estimations of Dimensions for Prestressed Concrete Bridges

Optimization of cross-section and non-prestressed reinforcement

Master's thesis in Master Programme Structural Engineering & Building Technology

ADAM ALJRAKI
MOHAMAD KHALOUF

Department of Architecture and Civil Engineering
Division of Structural Engineering
Concrete Structures

CHALMERS UNIVERSITY OF TECHNOLOGY
Gothenburg, Sweden 2022
www.chalmers.se

MASTER'S THESIS ACEX30

Early Estimations of Dimensions for Prestressed Concrete Bridges

Optimization of cross-section and non-prestressed reinforcement

Master's Thesis in the Master's Programme Structural Engineering and Building Technology

ADAM ALJRAKI
MOHAMAD KHALOUF

CHALMERS
UNIVERSITY OF TECHNOLOGY

Department of Architecture and Civil Engineering
Division of Structural Engineering
Concrete Structures
CHALMERS UNIVERSITY OF TECHNOLOGY
Göteborg, Sweden 2022

Early Estimations of Dimensions for Prestressed Concrete Bridges

Optimization of cross-section and non-prestressed reinforcement

Master's Thesis in the Master's Programme Structural Engineering and Building Technology

ADAM ALJRAKI

MOHAMAD KHALOUF

Examensarbete ACEX30
Institutionen för arkitektur och samhällsbyggnadsteknik
Chalmers tekniska högskola, 2022

Department of Architecture and Civil Engineering
Division of Structural Engineering
Concrete Structures
Chalmers University of Technology
SE-412 96 Göteborg
Sweden
Telephone: + 46 (0)31-772 1000

Cover:
Picture of studied two-span continuous prestressed concrete bridge.

Department of Architecture and Civil Engineering
Göteborg, Sweden, 2022

Early Estimations of Dimensions for Prestressed Concrete Bridges
Optimization of cross-section and non-prestressed reinforcement
Master's thesis in the Master's Programme Structural Engineering and Building Technology

ADAM ALJRAKI

MOHAMAD KALOUF

Department of Architecture and Civil Engineering
Division of Structural Engineering
Concrete Structures
Chalmers University of Technology

ABSTRACT

In bridge design, an early estimation of the dimensions and reinforcement content is made to estimate the cost of the bridge. The estimation is generally based upon experience and simplified calculations. From a sustainable as well as economic perspective, it is important to optimize the structures to reduce the environmental impact.

This master thesis is a continuation of the work by Aspegren & Möörk (2021) where the prestressed reinforcement was studied. In this master thesis the design will be expanded to also include non-prestressed reinforcement. For optimization, the set-based parametric design method is used in this thesis. It was implemented by further developing a python script by Aspegren & Möörk (2021). In the optimization, the beam height and amount of non-prestressed reinforcement was optimized with the aim to minimize the global warming potential (GWP) and construction cost, respectively, for the superstructure. This work facilitates a more efficient design of continuous prestressed concrete bridges in early stages, that will enhance sustainability and reduce costs instead of designing based on experience and simplified estimations only.

The study shows that higher beam heights generally give smaller amount of non-prestressed reinforcement and more optimal solutions with respect to (GWP). However, with the material costs used in the study, the beam height has no significant influence on the investment cost.

The potential for more efficient bridge designs were shown in a case study of an existing bridge. The optimization resulted in bridge solutions with approximately 10% reduced cost and 15% reduced GWP.

Key words: Prestressed concrete bridge, Preliminary design, Set-based parametric design, BRIGADE/Plus, non-prestressed reinforcement, Optimization

Contents

Preface

This study has been executed in the master's thesis course ACEX30 during the spring term, 2022, at the Department of Architecture and Civil Engineering of Chalmers University in collaboration with inhouse Tech Göteborg.

Firstly, we would like to give our appreciation to our Supervisors, Oscar Yman and Max Fredriksson from Inhouse Tech Göteborg AB, for providing assistance, support, and essential skills in structural engineering constantly during ambit of the course. We want to give our gratitude to Isak Svensson at Inhouse Tech Göteborg AB for python support, guidance.

Secondly, We would like to show our thankfulness for inhouse Tech Göteborg, for giving us the privilege of working with this thesis in their office in Gothenburg and providing us the hardware and software required in this thesis.

Finally, we would give a special thanks to our examiner Professor Mario Plos for his great ambition and patience in the project and his feedback during the course.

The Authors, Gothenburg, June 2022

List of Figures

List of Tables

Abbreviations

3D	Variable notation for something
ALS	Accidental limit state
CO_2	Carbon dioxide
CO_2-eq	Carbon dioxide equivalents
DOF	Degrees of freedom
EC	Eurocode
EPD	Environmental product declaration
GWP	Global warming potential
LM	Load model
SEK	Swedish crowns
SLS	Service limit state
STR	Internal failure or large deformations in the structure or structural parts where the material strength is decisive.
ULS	Ultimate limit state

Notations

Roman upper-case letters

A_{ct}	Concrete area in the tensile zone
A_c	Concrete area
A_P	Cross-section area of the prestressing steel
$A_{s.h}$	Horizontal non-prestressed reinforcement
$A_{s.l}$	Longitudinal non-prestressed reinforcement
$A_{s.min}$	Minimum cross-section area of reinforcement
$A_{s.v1}$	Torsional stirrups
$A_{s.v2}$	Shear stirrups
$A_{s.I}$	Longitudinal non-prestressed reinforcement
B_{es}	Width of the end-shield
E_c	Modulus of elasticity for the concrete
E_{cm}	Scant Modulus of elasticity for the concrete
E_p	Modulus of elasticity for prestressing steel
E_s	Design value of modulus of reinforcement steel
F_c	Resultant concrete force
F_{cd}	The design value of tensile force in the longitudinal reinforcement
F_{cs}	Shrinkage force
F_{cw}	Inclined resultant concrete force
F_s	Resultant steel force
F_{sv}	Vertical resultant steel force
F_{td}	The design value of tensile force in the longitudinal reinforcement
F_p	Force in the prestressing steel

$G_{k.j}$	Characteristic permanent load
H_l	Height of end-shield
I	Moment of inertia
K_0	Coefficient for earth pressure at rest
K_p	Coefficient for passive earth pressure
L	Total length of bridge
L_0	Distance from the support to where the tendon is at the same level as the centre of gravity of the cross-section
L_{CG}	Distance from the bottom of the beam to the centre of gravity
L_{ww}	Length of wingwalls
M_{ED}	Design moment
M_P	Primary moment
M_{RD}	Moment capacity
M_S	Secondary moment
N_{ed}	Axial force in the cross-section due to loading or prestressing.
P	Prestressing force
P_K	Characteristic value of a prestressing action
$P_{0\infty}$	Initial effective prestressing force.
P_∞	Tendon force after long time in the prestressing steel
$T_{Shrinkage}$	Temperature change to represent the shrinkage
Q_k	Characteristic point load
$Q_{k.1}$	Main characteristic variable load
$Q_{k.i}$	Characteristic variable load
R	Reaction force
S	First moment of area of the cross section
T_{Ed}	Design torsional moment
$T_{Rd,c}$	Design torsional cracking moment
$T_{Rd,max}$	Design torsional resistance moment
V_{ccd}	Transverse component (design value) of the compressive resultant
V_{Ed}	Total shear force from transverse load (Load effect), design value
$V_{Ed.net}$	The design shear force that should be resisted by the web
V_{td}	Transverse component (design value) of the tensile resultant
V_{ipd}	Transverse component (design value) of inclined prestressing force
$V_{Rd,c}$	Shear resistance in members without shear reinforcement
$V_{Rd,max}$	The upper limit of the shear resistance against the web shear compression failure for members with vertical shear reinforcement
$V_{Rd,s}$	Shear resistance against shear sliding failure for members with vertical shear reinforcement
W	Weight for each axel force
W_q	Weight for uniform distributed load in square meter
Z_H	Horizontal lever arm
Z_V	Vertical lever arm
Z	The inner lever arm for a member

Roman lower-case letters

b	Width of concrete section
b_w	Width of beam web

cc_{duct}	Centre to centre distance between tendon ducts
c_{min}	Minimum value of cover concrete
c_{nom}	Nominal concrete cover
d_{gg}	Maximum size of the aggregate
d_p	Distance from top of the beam to the centre of the prestressing steel
e	Eccentricity of the tendon from the centre of gravity
e_{span}	Maximum eccentricity of the tendon in the span
f_{cd}	Design compressive strength of concrete
f_{ck}	Characteristic compressive strength of concrete
f_{ctm}	Mean tensile strength of concrete
$f_{ct.eff}$	Tensile strength of concrete when cracking occurs. Set to fctm or lower (fctm(t)) if cracking occurs before 28 days after cast.
$f_{p.0,1k}$	Characteristic 0,1% strain limit for prestressing steel
f_{pd}	Design tensile capacity of prestressing steel
f_{pk}	Characteristic tensile capacity of prestressing steel
h	Height of the concrete section
k	Coefficient that compensates the impact of uneven residual stresses in the cross-section before cracking and change of internal level arm
k_c	Coefficient that considers stress distribution in the cross-section before cracking
l	Theoretical span length
n_1	Number of load fields
n_b	Number of bars in bundle
n_{tendon}	Number of tendons
q_k	Characteristic distributed load
t_{eif}	Effective wall thickness
z	Depth from zero-pressure level
z_i	Side length of the wall

Greek letters

α	Angle between the shear reinforcement and the beam axis perpendicular to shear forces
α_Q	Adjustment factor
α_{Qi}	Adaption factor for concentrated loads
α_{qi}	Adaption factor for distributed loads
α_{span}	Factor to decrease the eccentricity of the tendon in the span
α_c	Thermal expansion coefficient for concrete
Υ_s	Safety partial factor for steel
Υ_{Gj}	Safety partial factor for permanent loads
Υ_Q	Safety partial factor for variable loads
Υ_p	Safety partial factor for prestressing force
Υ	Density of the earth
δ	Horizontal movement of the bridge
δ_{max}	Maximum horizontal movement
$\Delta\varepsilon_p$	Strain in the tendons due to load effect

ε_{cs}	Shrinkage strain of concrete
ε_{p0i}	Initial strain of the prestressing steel
ε_{p}	Total strain in tendon
ε_{p0i}	Initial strain of the prestressing steel
ε_{p0}	Strain in the tendons due to prestressing
ε_{cu}	Strain in concrete
ξ_j	Reduction factor
θ	Inclination angle
Θ_d	Diameter of the bar
Θ_n	Equivalent diameter
μ	Frictional coefficient
$\rho_{w,min}$	Minimum ratio shear reinforcement
σ_S	Absolut value of the stress in the reinforcement after cracking. Not larger than the yield stress, fyk
$\sigma_{P.max}$	Maximum stress in the prestressing steel
$\sigma_{P.m0}$	Stress directly after the release of the tensioning the maximum
σ_{CC}	Concrete compressive stress
σ_{Cp}	Concrete stress at the level of prestressing steel
σ_{Ct}	Concrete tensile stress
χ_∞	Relaxation factor after long time
Ψ_0	Load combination factor
Ψ_0, i	Load combination factor for variable loads
Ψ_1	Load combination factor for frequent variable load
Ψ_2	Load combination factor for quasi-permanent variable load

1 Introduction

1.1 Background

On a global scale, the construction industry causes annually 23% of world's carbon dioxide (CO2) emissions according to Gao, et al. (2021). Large amounts of greenhouse gases are produced by the heavy steel and cement industry contributing together with a total of 15% of the world CO2 emissions (Ruijven, 2016). Boverket (2021) showed that the Swedish construction and real estate sector caused a total of 21% of greenhouse emissions in 2019. To cope with the net-zero emissions goal that has been set until 2045, strategies of material efficiency and circular economy has been adapted by the Swedish government (Energimyndigheten, 2021). It is therefore of great interest to optimize structures and minimize material use to meet the environmental goals.

In early phases of bridge design, an estimation of the dimensions and reinforcement amounts are made in order to predict the cost of the bridge. These estimations are normally based on experience and simplified calculations. The dimensions decide the amount of material used in the bridge and are usually not further developed in the detailed design phase. This means that the amount of material used in the bridge is mostly based on early estimations. This is not beneficial from a sustainable and economic perspective, since it usually is possible to find more optimal designs. Thus, the industry needs to find more effective methods and techniques to improve design accuracy in an early stage.

Aspegren & Möörk (2021) studied design optimization of continuous prestressed concrete bridges. The bridge type studied was a two-span prestressed concrete beam bridge consisting of a main beam (T-section), end-shields, wingwalls and supports, as shown in Figure 1.1. However, in their design optimization the non-prestressed reinforcement required for bending, shear and torsion in ultimate limit state was not included in the design.

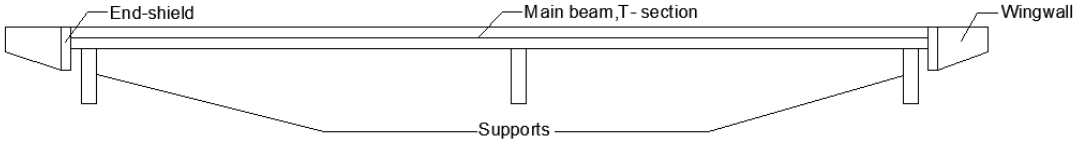

Figure 1.1 Structural members of the studied bridge based on Aspegren och Möörk (2021).

1.2 Aim and objectives

The aim of this master's thesis is to optimize the estimations of dimensions made for prestressed concrete bridges in an early stage of the design process. This thesis is a continuation of the work by Aspegren & Möörk (2021). Here, the design will be extended to also include non-prestressed reinforcement, so that also this can be included in the optimization. This will lead to a more efficient design that enhances sustainability and reduces costs instead of only depending on experience and simplified estimations.

To reach the aim, the following objectives have been identified for the project:

- To further develop an existing parametric design tool that generates the finite element (FE) model for structural analysis, previously developed by Aspegren & Möörk (2021).

- To design the cross-section and reinforcement needed for shear, torsion, and anchoring of the reinforcement in addition to the prestressing reinforcement, based on the section forces from the FE model.
- To determine the optimized combination of amount of concrete, non-prestressed and prestressed reinforcement, with respect to cost and carbon dioxide emissions, respectively.
- To evaluate the results obtained with the parametric design tool and compare to existing bridges.
- To evaluate different bridge geometries in order to find the most optimal bridge design for different span lengths.
- To draw conclusions from these results from both an environmental and economic perspective.

1.3 Limitations

- The design concerns post-tensioned concrete beam bridges in two spans only.
- In the optimization, standard values for cost and environmental impact of the materials are used according to Eurocode (SIS, 2002a) and Swedish Transport Administration (Trafikverket, 2019a). The possibility to use material with better performance is not taken into account.
- The use of different design standards may alter the results slightly.
- The calculation of bending moment is not included in this study.

1.4 Methodology

The master thesis starts with studying the theory and literature concerning prestressed concrete bridges, parametric design and optimization with respect to environmental impact and economy. To get a good understanding of the design procedure in an early stage, the standardized design method for this type bridges is studied by interviews of experienced structural engineers. It is essential to understand different types of reinforcement in the bridge and how different parameters are related to each other. Once all important parameters are identified the second part of the project can start.

The design procedure starts with further developing of an existing python script that can be connected to the design software, BRIGADE/Plus (Scanscot Technology, 2021), in which the FE model is defined. The FE model including the structural components of the bridge, reinforcement, loads, boundary conditions, as well as the span length, width and beam height are built and controlled by the script. The combination between Python and the design software gives the opportunity to optimize reinforcement needed for bending, shear, torsion, and other bridge parameters. BRIGADE/Plus (Scanscot Technology, 2021) is used as a plug-in to the general FE software Abaqus, where the analysis of the structure is taking place. In the FE model assumptions and choices are made for structural parts and other parameters in order to simplify the complexity of the structure.

In the parametric design, the relation between the beam height and quantities of bending, shear and torsion reinforcement is optimized for bridges with different spans and widths. The reinforcement arrangement influences the structural behavior of the

bridge as well. To study the combinations of these sets of parameters a set-based parametric design is used. The applied method is used to achieve the most efficient solution based on two optimization criteria i.e., environmental and economic.

The first criteria, environmental impact, is evaluated by global warming potential (GWP) and the second criteria is evaluated by the material cost of the bridge. Values of the GWP, cost of the materials as well as initial dimensions of the studied bridges are based on the previous master thesis by Aspegren & Möörk (2021). Since the tendon layout of the prestressed reinforcement and beam height in relation to the optimization criteria have been covered by Aspegren & Möörk (2021), the major focus in this thesis will be on non-prestressed reinforcement with respect to the parameters mentioned.

The FE analysis is used for the system analysis, while the design checks and calculation of necessary non-prestressed reinforcement are made using the cross-sectional forces from the FE analysis. The design method is applied to prestressed concrete bridges in two spans, which are assessed by comparing the resulting design with existing bridges. This gives the opportunity to see if a more optimal design can be reached with respect to environment impact and investment cost.

2 Design of prestressed concrete beam bridges

In this chapter, both the theory and the current design process of prestressed concrete bridges are described.

2.1 Continuous post-tensioned bridges

In this thesis, prestressed continuous post-tensioned concrete bridges with two spans are studied. In post-tensioning, the concrete is cast first and the steel is tensioned afterward. According to Engström (2011) different methods are used to insert the prestressing steel in the ducts. The prestressing steel can be inserted in the duct already when it is placed in the casting form. Another method is to mount the empty ducts first and pull the tendons into the ducts after the concrete is cast. The tensioning can be applied once the concrete has achieved 70% of its 28-day's strength. Hydraulic jacks are used to apply the required tensile force to the prestressing steel. During the tensioning operation, the tensile force and free elongation of the tendon are measured and compared with predicted values. The free elongation of the tendon is based on both the compression deformations in the concrete, and the elongation of the prestressed steel. After the tensioning operation the ducts are filled with grout in order to achieve full interaction between the concrete and the prestressed steel. Moreover, the grout is used to protect the steel from corrosion. After grouting, any change of the strain for the prestressed steel and the concrete will be the same, at the same level of the cross section.

Design of prestressed concrete is more complex than of plain and reinforced concrete and Eurocode deals with prestressing effects by additional loads and other specific conditions to the prestressed member, Engström (2011). The strain compatibility approach and the tendon force approach are two ways of designing prestressed concrete structures. Each of these approaches have different advantages and require some conditions for them to be applied. An advantage with the strain compatibility approach is that it is the traditional method that is also used for normal reinforced concrete, and is based on equilibrium, compatibility and constitutive relations. However, this approach can only be used in the case of full interaction between concrete and prestressing steel. Table 2.1 shows the most common cases where each of these approaches can be used.

Table 2.1 Applications of Tendon Force and Strain Compatibility approaches according to Engström (2011).

Tendon Force Approach Can always be used, but is needed for:	**Strain Compatibility Approach Full interaction between steel and concrete is needed. Can be used for:**
Post-tensioning before grouting	Post-tensioning after grouting
Systems without bond	Pre-tensioning
External prestressing	-

The strain compatibility approach assumes that the prestressing steel is a part of the cross-section contributing to its resistance to loads, Engström (2011). However, this is not the case in the tendon force approach where the prestressed steel is considered as a separate unit acting externally on the structural member. Consequently, prestressing steel adds to concrete cross sectional resistance in the first approach but noy in the

second. For both the strain compatibility and the tendon force approach, initial and after loading concrete stresses are stated in Equations (2.1) and (2.2), respectively. To describe the concrete stress in a centrically loaded prestressed concrete prism.

$$\sigma_{ci} = \frac{-P_{0,i}}{A_I} \quad (2.1)$$

$$\sigma_c = \frac{-P_{0,i}+N}{A_I} \quad (2.2)$$

σ_{ci} Initial concrete stresses.

$P_{0,i}$ Initial effective prestressing force.

N External tensile force.

A_I $A_I = A_c + (\alpha_p - 1)A_p + (\alpha_s - 1)A_s$ (2.3)

α_p $\alpha_p = \frac{E_p}{E_{cm}}$ (2.4)

α_s $\alpha_s = \frac{E_s}{E_{cm}}$ (2.5)

A_c Area of gross concrete section

A_I Area of transformed concrete section

A_p Area of prestressing steel

E_p Modulus of elasticity of prestressing steel

E_{cm} Secant modulus of elasticity of concrete

E_s Design value of modulus of reinforcement steel

2.1.1 Influence of prestressing

The main idea with the prestressing is to add compression to prestressed member in order to delay or prevent cracking, Engström (2011). Consequently, the purpose of prestressing is to improve the service behavior. Since the cracking is delayed or prevented, many positive effects are obtained for the prestressed member. Since the concrete is in compression until cracking is reached (State I behavior), it will show an increased stiffness. As a result, fewer supports and longer spans can be used. An additional positive effect of prestressing is a reduced risk for corrosion, and smaller fatigue stresses. Increasing of the stiffness due to prestressing can generate more slender members. The approximate maximum span to length ratio is $\frac{l}{h} = 28$ for reinforced concrete beam bridges (with cracked sections in state II under service loads) while the approximate ratio is $\frac{l}{h} = 45$ for prestressed member (with uncracked sections in state I under service loads).

During the tensioning operation frictional forces occur in post tensioned structures between the ducts and the tendons, Engström (2011). That is due to intended changed in inclination of the tendon profile, as well as the unintended curvature, as shown in Figure 2.1. The unintended curvature takes place in the tendon duct and occurs because of the variation in the way of fixing the duct in the formwork.

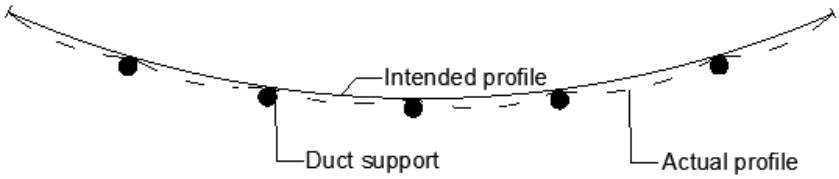

Figure 2.1 *Intended tendon profile and the actual curve for the tendon duct. Based on Engström (2015).*

The tendon force will vary along the beam due to frictional losses between the tendon and the duct, Engström (2015). The frictional losses are proportional to the intended curvature of the duct, with a uniform addition from the unintended curvature. As a result, the tendon force will decrease along the beam, measured from the jack end, as shown in Figure 2.2.

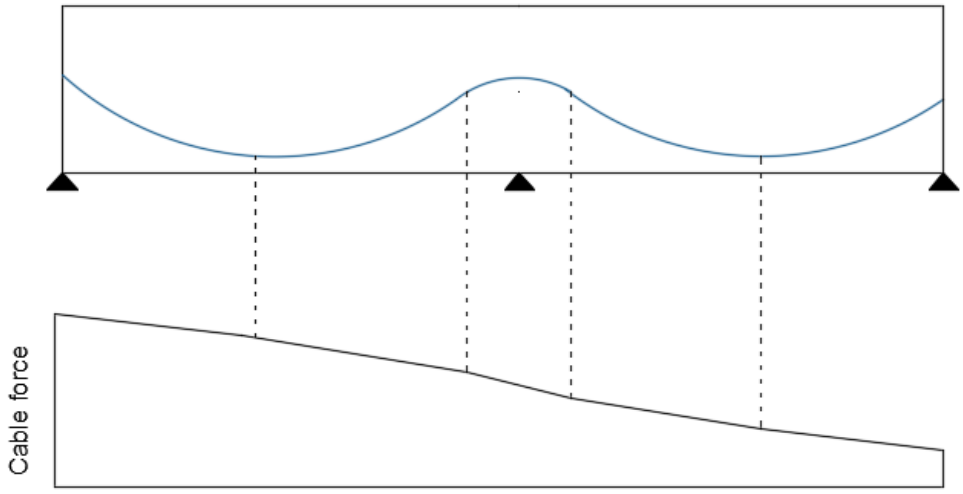

Figure 2.2 *Variation of tendon force in post-tensioned beam with the active end for tensioning to the left. Based on Engström (2015).*

According to Engström (2015), the effective prestressing force can be calculated as stated in Equation (2.6).

$$P_i(s) = P_i(0) * e^{-\mu(\alpha + k*s)} \quad (2.6)$$

$P_i(0)$ Tendon force at the end where the jack is placed.

α Accumulated nominal change of slope.

μ Frictional coefficient.

k Unintended angular displacement per unit length.

2.1.2 Bending moments

In design of prestressed beams, the moments are divided in fundamental and secondary moments. Fundamental moments are effects of external loads acting on the beam and can be calculated based on tables for continuous beams.

Secondary moments in concrete structures occurs if free deflections are prevented by restraints. In continuous prestressed concrete beams, the eccentricity of the tendon is a major action causing a secondary moment, Engström (2015). The eccentricity of the tendon normally gives rise to support reactions, if lifting at intermediate supports are prevented. These support reactions will, in turn, generate a secondary moment. As a result of this restraint moment, the moment at mid-span will reduce and therefore deflections can decrease. According to Eurocode (SIS, 2005a) the restraint moment should be taken into account for serviceability limit state (SLS) as well as for ultimate limit state (ULS). In SLS, the restraint moment depends on the stiffness and stiffness distribution in the beam. For ULS, the restraint effect differs between non-prestressed reinforced and prestressed concrete beams. In reinforced concrete beams, the restraint moments due to temperature, and shrinkage are generally small and will eventually disappear due to plastic redistribution. However, in case of limited plastic rotation capacity, the restraint moments need to be taken into account. For prestressed concrete beams, a large restraint moment is generated due to the eccentricity of the prestressing force, and due to the limited ductility, the design cannot rely on plastic redistributions. Due to these conditions, it is conservative to include the full restraint moment in the ULS for prestressed concrete.

Concrete beam bridges that consist of two symmetrical spans can be subjected to different load combinations which in turn affect the continuity condition. In the case of a load combination where the permanent load is applied in both spans while the variable loads are applied in one span, the continuity condition will be as expressed in Equation 2.7, Engström (2015). In a load combination where both permanent and variable loads are applied in both spans the continuity condition will be as expressed in Equation 2.8. The support moment at the mid support is solved by these continuity conditions stated earlier by superposition of the contribution from the different loads acting on the beam. All loads presented in Table 2.2 will have a contribution to the continuity condition.

$$\Theta_{B1} + \Theta_{B2} = 0 \tag{2.7}$$

$$\Theta_{B1} = \Theta_{B2} = 0 \tag{2.8}$$

Table 2.2 Mid-support rotation angles for different moment distributions caused by different loads. Based on Engström (2015).

Loads	**Moment distribution**	**Mid-support rotation**
Equally distributed loads	Parabolic	$\frac{q * l^3}{24EI}$
Restraint Moment	Triangular	$\frac{M * l}{3EI}$
Thermal (Shrinkage)	Constant	$-\frac{\alpha_c * \Delta T l}{2h}$

Prestressing	Specific for every case	$\frac{1}{l} * \int_o^l \kappa_p(x) * x dx$
Point load	Triangular	$\frac{q * l^2}{16EI}$

2.1.3 Concrete cover

Eurocode (SIS, 2005a) defines the concrete cover as the minimum distance between the surface of the reinforcement and the nearest surface of concrete. The nominal concrete cover, c_{nom}, consists of a minimum value of cover concrete, c_{min}, and the allowable deviation, Δc_{dev} , as stated in Equation (2.9).

$$c_{nom} = c_{min} + \Delta c_{dev} \tag{2.9}$$

The maximum allowable deviation Δc_{dev} for reinforced concrete is 10 mm, Eurocode (SIS, 2005a). The concrete cover provides protection to the reinforcement from weather conditions to decrease corrosion risk. More functions of the concrete cover are to provide fire protection and safely transfer bond forces between concrete and reinforcement. The maximum value of the minimum cover thickness should be chosen according to the bond demands and environmental impact, as stated in Equation (2.10).

$$c_{min} = max \begin{cases} c_{min,b} \\ c_{min,dur} \\ 10mm \end{cases} \tag{2.10}$$

$c_{min,b}$ Minimum value of cover thickness with regard to bond demand.

$c_{min,dur}$ Minimum value of cover thickness according to environmental impact.

The value of $c_{min,b}$ depends on the reinforcement arrangement of the bars and the aggregate size. In case of separated and bundled bars the diameter bar and an equivalent diameter is chosen respectively in accordance with Eurocode 2 (SIS, 2005a). When the nominal maximum aggregate size is equal to or larger than 32 mm $c_{min,b}$ should be increased by 5 mm as stated in Equation (2.11)

$$c_{min,b} \geq max \begin{cases} c_{minb} \\ \Theta_d \\ \Theta_n \end{cases} \tag{2.11}$$

Θ_d Diameter of the bar.

Θ_n Equivalent diameter of the bar, expressed by Equation (2.12).

$$\Theta_n = \Theta_d * \sqrt{n_b} \leq 55mm \tag{2.12}$$

n_b Number of bars in bundle

$$n_b \leq 4 \quad \text{During compression for vertical bars.} \tag{2.13}$$

$$n_b \leq 3 \quad \text{For all other cases.} \tag{2.14}$$

Transportstyrelsen (2018) specifies the concrete cover thickness $c_{min,dur}$ with respect to service life, water cement ratio and exposure class Furthermore, the covers should be increased by 10 mm for reinforcement that is sensitive for corrosion, including post-tension reinforcement Moreover Trafikverket (2019a) demands the minimum value of the cover thickness for bridge with service life 80 years to be 25mm, nevertheless this

value increases for corrosion sensitive reinforcement that are placed on the top of the bridge beams to 45mm. However, the used cover thickness is according to Transportstyrelsen, (2018) where the requirements for the cover thickness are more cautious than Trafikverket (2019a). These demands can be clarified in Equations (2.15), (2.16). with respect to deviations.

$$c_{nom} - \emptyset_{stirrups} \geq 35mm \tag{2.15}$$

$$c_{n.top} - \emptyset_{stirrups} \geq 55mm \tag{2.16}$$

$c_{n.top}$ The nominal cover thickness on the top side of the beam bridge.

Beside to cover thickness demands, the vertical and horizontal spacing between the bars is clarified in (SIS, 2005a), and it can be expressed as in Equation (2.17) and figure 2.3

$$a_s \geq max \begin{cases} \emptyset_{stirrups} \\ d_{gg} + 5mm \\ 20mm \end{cases} \tag{2.17}$$

d_{gg} Maximum size of the aggregate.

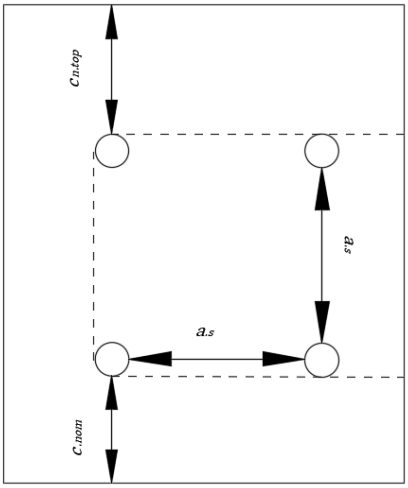

Figure 2.3 Simplified sketch that shows the cover thickness and spacing between the rebars in a reinforced concrete section, based on (SIS, 2005a).

2.2 Loads

Since the studied bridge is a concrete road beam bridge, the design should be in accordance with Eurocode, and Trafikverket (2019a). Whereas this thesis is studying the superstructure of the bridge, only the loads applied on the superstructure parts of the bridge should be included. The same load requirements as in the previous master thesis, Aspegren & Möörk (2021), are used. In the design procedure there are still many loads to account for:

Permanent loads

- Permanent load comprises of the self-weights of the beams, the bridge slab, the 100 mm pavement, the end-shields and wing-walls.

- Due to the connection between the end-shields and the main beam, the horizontal pressure on the end shields will affect the main beam as well, and can increase the moment and shear force
- Support settlements should be included since uneven settlements under the supports can generate forces in the beam.

Variable loads

- Traffic loads according to Eurocode (SIS, 2003a)
- Acceleration force was included as a longitudinal force on the surface of roadway, according to Eurocode (SIS, 2003a)
- Earth pressures increases due to the surcharge load, which can increase the moment and normal force.
- As described in section 2.1.2 the temperature has an effect and can generate restraint moment, since the beam can elongate and increase the earth pressure on the end-shield.
- Transverse loads as the wind loads are applied on both bridge and on the vehicles. The wind load can generate both bending and torsional moment on the bridge superstructure.

2.2.1 Traffic loads

In Sweden, bridges should be designed for traffic load models based on both Eurocode (SIS, 2003a) and Trafikverket (2019b). In this thesis, the bridge is designed for load model LM1 according to Eurocode as well as for the national vehicle models. The rest of the load models in Eurocode will not be included in order to reduce the complexity in the study. Figure2.4 describes how the bridge deck is divided into different load fields (with widths w1) based on the total width of the carriageway.

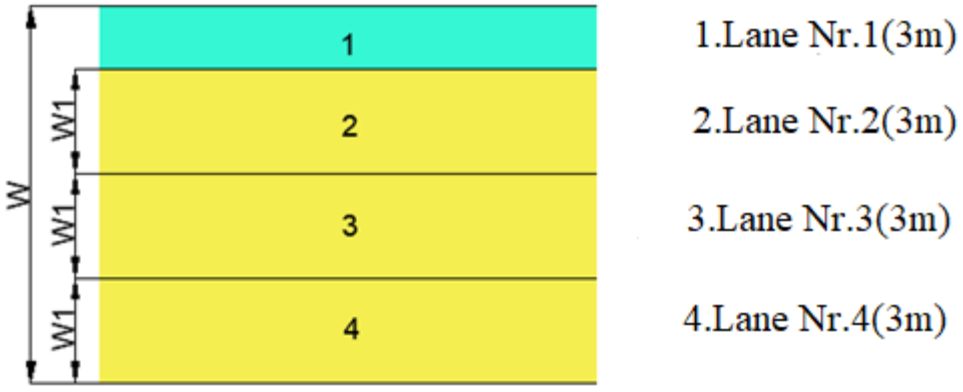

Figure 2.4 Placement of load fields according to Eurocode (SIS, 2003a).

Load model 1

Load model 1 consists of both concentrated loads from two axles (tandem system) and a uniformly distributed load (UDL), see Figure 2.5. For the tandem system the weight for each axle is specified in Equation (2.18).

$$W = Q_k * \alpha_Q \quad (2.18)$$

W Axle force.

Q_k Axle load according to Eurocode (SIS, 2003a).

α_Q Adjustment factor, based on Transportstyrelsen (2018).

In (SIS, 2003a) the following requirements should be followed:

- One tandem system for every notional lane
- Loads for each wheel is half of weight for each axle.
- Contact surface area for every wheel is $0.4m^2$.
- Each vehicle load is placed symmetrically about the longitudinal axis of the load field.

The uniformly distributed load is stated in Equation (2.19).

$$W_q = q_k * \alpha_Q \quad (2.19)$$

W_q Uniformly distributed load per square meter.

q_k Distributed load.

The distributed load should be applied in the unfavourable parts of the affected surface. See Figure 2.5

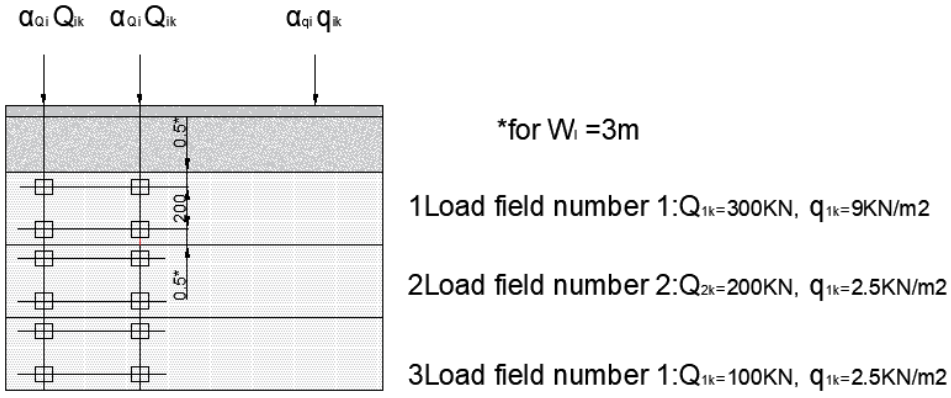

Figure 2.5 Load placement in LM1 according to Eurocode (SIS, 2003a).

National Vehicle model

There are different load cases described in Trafikverket (2019b), that should be positioned in the most unfavourable placement. The placement of vehicle can be in two fields with loading factor of 1.0 and 0.8. In case when there are more than two load fields are applied then the other fields are subjected to uniform loads of 0 or 5kN/m Transportstyrelsen (2018).

2.3 Preliminary Design

Today, in an early stage of the design process, dimensions of concrete members are assumed or guessed based on experience by the designer. Then, sectional forces are determined from the loads acting on the member, after which the reinforcement can be designed. The design procedure consists also of checks that requirements

according to Eurocode (SIS, 2005a) and additional regulations from Trafikverket (Trafikverket, 2019a) are fulfilled.

Prestressing concrete structures induces a major difference in the preliminary design approach, according to Bhatt (2011). In general, prestressed concrete structures are designed to resist load actions in SLS, and ULS checks are performed to satisfy general safety requirements. Reinforced concrete structures, on the other hand, are designed in ULS to begin with, and SLS requirements are checked after that. According to Engström (2011), the design choices concerning the prestressing force and its eccentricity are made to fulfill criteria in SLS regarding three main design conditions: limitation of deflections, of crack formation and of support rotations, at a different loads and for different requirements. To express these conditions in a simplified manner, stresses are studied and limited to specific values.

2.3.1 Prestressing and reinforcement steel

In the previous thesis by Aspegren & Möörk (2021), the preliminary design with respect to prestressed reinforcement have been studied, including the layout and number of tendons. However, the non-prestressed reinforcement was not accurately designed, but instead recommended minimum values from Eurocode and Trafikverket were used. Eurocode (SIS, 2005a) recommends the minimum reinforcement in tensile zones for profiled cross sections, such as T-sections, determined individually for the web and the flange, respectively, according to Equation (2.20).

$$A_{s,min.EC}\sigma_s = k_c k f_{ct,eff} A_{ct} \tag{2.20}$$

$A_{s,min.EC}$ Minimum cross-section area of reinforcement in tensile zone according to Eurocode.

σ_s Stress in the reinforcement after cracking. Should not be larger than the yield stress, f_{yk}.

k_c Coefficient that considers stress distribution in the cross-section before cracking.

k Coefficient that compensates the impact of uneven residual stresses in the cross section before cracking and change of internal lever arm.

$f_{ct,eff}$ Effective concrete tensile strength. Should not be higher than f_{ctm} (or $f_{ctm}(t)$) if the check of cracking is made before 28 days after casting).

f_{ctm} Mean tensile strength of concrete.

A_{ct} Concrete area in the tensile zone.

The Swedish regulations Trafikverket (2019a) have an additional requirement regarding the minimum amount of reinforcement according to Equation (2.21).

$$A_{s,min} = \min\left(4.0\frac{cm^2}{m}, 4.0 * \frac{f_{ctm}}{3}\frac{cm^2}{m}, \rho_{min} * A_c, A_{s,min.EC}\right) \tag{2.21}$$

$A_{s,min}$ Minimum cross-section area of reinforcement.

A_c Concrete cross-sectional area.

ρ_{min} 0.08 if b_w/ h > 5, otherwise 0.05.

2.3.2 Load combinations

In Eurocode (SIS, 2005a), load combinations for structures are performed both in ULS and SLS. Load combinations for permanent and variable loads are performed where it is investigated if the loads have a favorable or unfavorable effect to get the most critical load combination. In ULS, verifications are made for fundamental load combinations, accidental design situations and seismic design situations, while in SLS they are made for characteristic load combinations, frequent load combinations and quasi-permanent load combinations. The Accidental Limit State (ALS) has been checked by Aspegren & Möörk (2021) and only fundamental load combinations are made for ULS in this thesis. In addition, all SLS load combinations are used to perform checks in various stages as presented in chapter 2.2.4.

2.3.3 Ultimate limit state

ULS is the basic limit criterion that handles the structures' safety and ensures that they resist the ultimate loads that may act on them, Bhatt (2011). In Eurocode (SIS, 2002b), ULS fundamental load combinations are made according to the design situation to the following categories:

- EQU: The structure or a component of it loses static equilibrium when considered as a rigid body.
- STR: The structure or any of its structural components reaches internal failure or major deformations where the strength of the materials is governing.
- GEO: The ground reaches failure or major deformations because the strength of soil or rock is exceeded.
- FAT: The structure or any of its structural components fails in fatigue.

In this thesis the STR is applicable, and the other categories are not used. Eurocode (SIS, 2002b) expressions for load combinations of the category STR is used as follows:

$$max \begin{cases} \sum_{j\geq 1} \gamma_{G,j} G_{k,j} \text{"} + \text{"} \gamma_P P \text{"} + \text{"} \gamma_{Q,1} \psi_{0,1} Q_{k,1} \text{"} + \text{"} \sum_{i>1} \gamma_{Q,i} \psi_{0,i} Q_{k,i} \\ \sum_{j\geq 1} \xi_j \gamma_{G,j} G_{k,j} \text{"} + \text{"} \gamma_P P \text{"} + \text{"} \gamma_{Q,1} Q_{k,1} \text{"} + \text{"} \sum_{i>1} \gamma_{Q,i} \psi_{0,i} Q_{k,i} \end{cases} \quad (2.22)$$

"+"	Means "To be combined with".
$\sum$	Means "The combined effect of".
$G_{k,j}$	Characteristic permanent load.
$\gamma_{G,j}$	Safety partial factor for permanent loads.
γ_Q	Safety partial factor for variable loads.
γ_P	Safety partial factor for prestressing force.
$\psi_{0,i}$	Load combination factor for variable loads.
$Q_{k,1}$	Main characteristic variable load.
$Q_{k,i}$	Characteristic variable load.
P	Prestressing force.
ξ_j	Reduction factor.

The permanent and variable load actions are represented by G and Q, respectively, and Eurocode (SIS, 2002b) defines a set of equations. Trafikverket (2019a) requires that set B is to be used for STR. The set B in Eurocode (SIS, 2002b) specifies the combinations of the partial safety factor γ and the reduction factor ξ as shown in Table 2.3. The partial factors for the permanent actions in the case of unfavourable and favourable load combinations have the values $\gamma_{Gj,sup} = 1{,}35$ and $\gamma_{Gj,inf} = 1{,}00$ respectively. The partial factor for the variable actions is $\gamma_{Q,1} = 1{,}50$ and the reduction factor is $\xi = 0{,}85$.

Table 2.3 STR Design values of actions used in set B. Based on Eurocode (SIS, 2002b).

STR	**Permanent actions**		**Leading variable action**	**Accompanying variable actions**	
	Unfavourable	Favourable	Action	Main	Others
Equation (2.22)	$\gamma_{Gj,sup}G_{kj,sup}$	$\gamma_{Gj,inf}\mathrm{G}_{kj,inf}$		$\gamma_{Q,1}\psi_{0,1}Q_{k,1}$	$\gamma_{Q,i}\psi_{0,i}Q_{k,i}$
Equation (2.22)	$\xi\gamma_{Gj,sup}G_{kj,sup}$	$\gamma_{Gj,inf}\mathrm{G}_{kj,inf}$	$\gamma_{Q,1}Q_{k,1}$		$\gamma_{Q,i}\psi_{0,i}Q_{k,i}$

Similar to columns, webs in T-sections are subjected to major compressive stresses because of the prestressing forces that are applied, Engström (2011). In ULS, these compressive stresses at the prestressing steel level should be calculated for initial stage and after long time, respectively, both in the strain compatibility approach and tendon force approach as in Equations (2.23) and (2.24), respectively.

$$\sigma_{cp} = \frac{\gamma_p P_{0\infty}}{A_c} \tag{2.23}$$

$$\sigma_{cp} = \frac{\gamma_p P_{\infty}}{A_c} \tag{2.24}$$

σ_{cp} Concrete stress at the level of the prestressing steel.

$P_{0\infty}$ Initial effective prestressing force.

P_{∞} Tendon force after long time in the prestressing steel.

γ_p Partial factor for prestress.

2.3.4 Service limit state

SLS is the basic limit criterion regarding serviceability and comfort of structures. It ensures that the applied loads are resisted without undesirable deflections, excessive crack widths or too much vibration, Bhatt (2011). In SLS the characteristic, frequent and quasi-permanent load combinations are presented in Equations (2.25) to (2.28).

The Characteristic (rare) combination is used for irreversible limit states:

$$\sum_{j\geq 1} G_{k,j}" + "P_k" + "Q_{k,1}" + "\sum_{i>1} \psi_{0,i}Q_{k,i} \tag{2.25}$$

The Frequent combination is used for reversible limit states:

$$\sum_{j\geq 1} G_{k,j}" + "P_k" + "\psi_{1,1} Q_{k,1}" + " \sum_{i>1} \psi_{2,i} Q_{k,i} \quad (2.26)$$

The Quasi-permanent combination is used for long term effects:

$$\sum_{j\geq 1} G_{k,j}" + "P_k" + "Q_{k,1}" + " \sum_{i>1} \psi_{2,i} Q_{k,i} \quad (2.28)$$

ψ_1 Load combination factor for frequent variable load.

ψ_2 Load combination factor for quasi-permanent variable load.

P_k Characteristic value of a prestressing action.

In design calculations for post-tensioned concrete, it is important to distinguish between three different stages, occurring at different ages of the structure; the stage of tensioning, the stage of applying the loads when the structure is put into service and the stage after long time. In these stages some specific limitations are more relevant, and some load cases are more critical and governing the design than others, Engström (2011).

At the stage of tensioning, Eurocode 2 limits the maximum tensile stress in the steel is according to Equation (2.29), Engström (2011).

$$\sigma_{p,max} = min \begin{cases} 0{,}9 f_{p0,1k} \\ 0{,}8 f_{puk} \end{cases} \quad (2.29)$$

$f_{p0,1k}$ Characteristic tensile capacity.

f_{puk} Characteristic 0,1% strain limit.

After tensioning and anchorage of the tendons as well as after long time, the prestressed steel stress is limited according to Equations (2.30) (Engström, 2011). For simplification and not to have to account for the non-linearity of concrete creep, the concrete compressive stress is limited according to Equation (2.31)

$$\sigma_{p,m0} = min \begin{cases} 0{,}85 f_{p0,1k} \\ 0{,}75 f_{puk} \end{cases} \quad (2.30)$$

$$|\sigma_{cc}| \leq 0{,}45 f_{ck} \quad (2.31)$$

After long time, crack formation needs to be controlled for the characteristic load combination (Engström, 2011). For fully prestressed members no crack formation is allowed, but in partial prestressing limited cracking is allowed for big loads, Engström (2011). If the bridge is exposed to severe conditions like exposure classes XD, XF and XS, it is appropriate to avoid longitudinal cracks and micro-cracks and concrete compressive stress is limited according to Equation (2.32).

$$|\sigma_{cc}| \leq 0{,}6 f_{ck} \quad (2.32)$$

Trafikverket (2019a) sets regulations on the allowable deformations of the bridge deck in SLS. For road bridges maximum deflections in both longitudinal and transversal direction should not be larger than $l/400$, where l is the theoretical span length. By defining the prestressing force and its eccentricity, cracks can be limited in order to reach a long service life, (Engström, 2011). Additionally, this definition can be used to achieve zero deflection in midspan for quasi-permanent loading.

2.4 Shear

To understand the behavior of shear in a structural element it can be divided into chords and struts as described in Eurocode (SIS, 2005a). Figure 2.5 represents a truss model for a shear reinforced element consisting of compression chord, struts, tensile chord and shear reinforcement. Engström (2011) explains how the shear forces can be resisted by the chords and shear reinforcement by the web. When the structural element has a variable depth, the compressed or the tensioned chord will be inclined as well. Consequently, the forces in these regions will be inclined and that affects the transverse equilibrium of the cross-section.

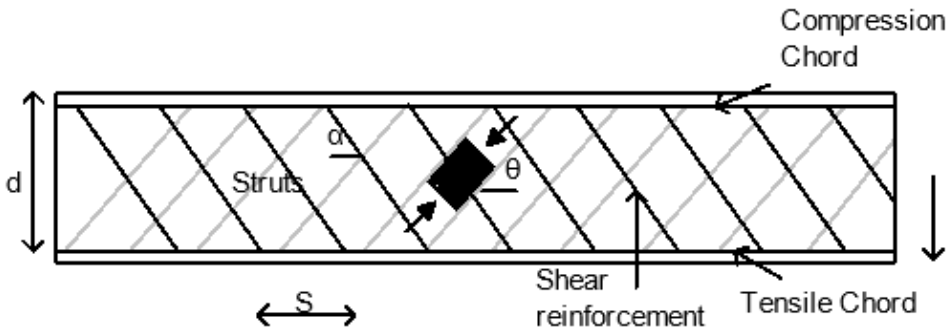

Figure 2.6 Shear reinforced members with relevant components according to Eurocode (SIS, 2005a).

2.4.1 Shear cracking in concrete members

Cracking of reinforced and prestressed structures is the stage that occurs before failure in which the structure losses its stiffness gradually. Normal and shear stresses in a reinforced member are influenced by the cracks and when loading structures in bending and shear, without prestress, these stresses will be distributed as in Figure 2.7, Engström (2011).

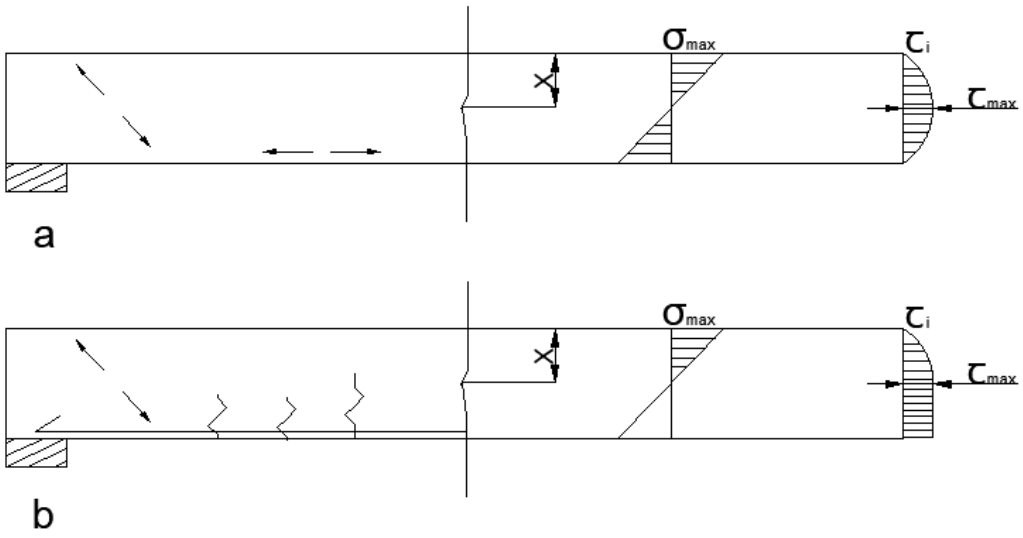

Figure 2.7 *The normal and shear stresses in reinforced concrete section generated due to shear and bending moment a) concrete section is uncracked (state I) b) concrete section is cracked with flexural cracks (State II). Based on Engström (2011).*

The first cracks initiate in the tensile edge when the principal tensile stress exceeds the concrete tensile strength, Engström (2011). The principal tensile stress at the lowest point of the cross section is parallel to the tensile edge; therefore, the initiated crack propagates perpendicular to the edge and is called a flexural crack. Towards the supports, normal stresses from bending are lower while shear stresses are higher. Because the principal tensile stress is influenced by both normal and shear stresses, it will change direction progressively over the height. In a beam without prestress or external normal force, close to the support, the shear stresses reaches its maximum value and the normal stresses are zero at centroidal axis. Here the inclination of the principal tensile stress σ_2 is 45° with the beam axis and can be calculated as in Equations below. Here, if the principal stress reaches the tensile strength, a web shear crack is formed.

$$\sigma_2 = \tau_{max} \tag{2.33}$$

$$\tau_{max} = \frac{V*S}{b_w*I} \quad \text{(In general)} \tag{2.34}$$

$$\tau_{max} = \frac{V}{b_w*z} \quad \text{(For rectangular cross-section)} \tag{2.35}$$

b_w Width of the web

S First moment of area of the cross section

I Moment of inertia of the cross section

z Internal lever arm

The flexural shear crack and the web shear crack are two types of cracks that occur because of the influence of shear. They are influenced by both the magnitude of the shear force and of how the origin of the crack, and they occur at different positions along the beam. The flexural shear cracks develop from flexural cracks that extends into regions of the cross-section with high shear forces; the cracks change direction due to the inclined principal tensile stresses, as shown in Figure 2.8. Depending on the

structure and loading condition, web shear cracks may occur in regions near to the exterior support where the shear stresses are high at the same time as the bending stresses are very low.

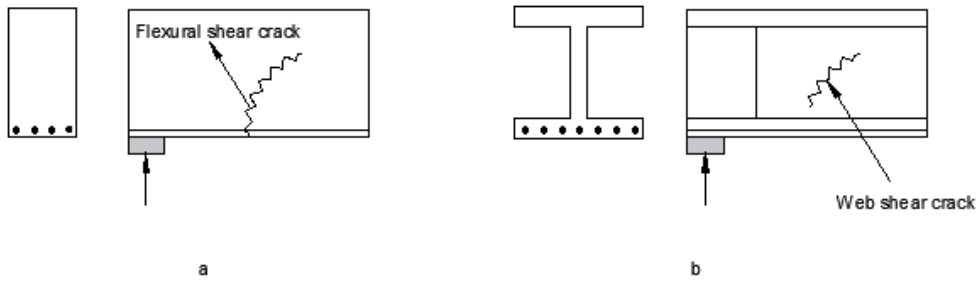

Figure 2.8 *a) Types of cracks in reinforced concrete members: flexural shear and flexural cracks, b) web shear crack. Based on Engström (2011).*

Prestressing of concrete structures results in stiffer elements with less deflections and delayed cracking which will lead to a safer design in ULS, Engström (2011). Both flexural cracks and flexural shear cracks are delayed in regions near to the simply supported ends because the critical tensile edge is still in compression. This means that the web shear cracking and shear sliding failure will likely not appear in these regions. Prestressing will also have an impact on the principal tensile stress which will lead to an inclination that is less than 45° for shear cracks, a smaller inclination in comparison with reinforced concrete.

2.4.2 Types of shear failure

When studying different types of shears failures, it is important to differentiate between if the structural member is provided with shear reinforcement or not. When increasing the load on a member without shear reinforcement, flexural cracks can develop and shear sliding takes place along the crack, Engström (2011). This type of failure is called shear sliding failure and is also known as flexural shear failure, see Figure 2.9a. The influence of prestressing on this failure is that it increases the capacity of the section due to the arch effect.

Various types of shear failures in reinforced and prestressed concrete can occur either in the concrete or in the reinforcement, Engström (2011). Some failures only occur in reinforced concrete members and other failures only in prestressed concrete members. In reinforced concrete, shear failure can occur due to the lack of capacity of the friction and interlocking forces. A type of failure, that occurs in reinforced concrete, is shear sliding failure with yielding reinforcement, see Figure 2.9b. The shear force in this case is lifted and taken by shear reinforcement or stirrups. Here, the inclination of the compressive strut depends on the arrangement and how much shear reinforcement is provided. In this failure, the shear reinforcement yields and for prestressed concrete the advantage of prestressing is not utilized.

Another type of failure that occurs in reinforced concrete is web shear compression failure where the crushing takes place in the inclined concrete strut, see Figure 2.9c. The influence of prestressing on this failure depends on if the prestressing is moderate or high. Moderate prestressing increases the capacity and high prestressing decreases

the capacity. The shear capacity of this failure usually governs the design of prestressed concrete members since the web in such structures is often optimized, Engström (2011). Web shear tension failure is a brittle failure that occurs instantly and can cause huge damage in members without shear reinforcement. This brittle failure takes place only in prestressed concrete members when concrete is exposed to high compression. Once the shear cracks occur in the web, concrete fails rapidly in an explosive manner. The web shear capacity is influenced by the level of prestressing and web shear cracks occur for a much higher shear force in prestressed members. Therefore, the cracks develop even faster in prestressed members compared to non-prestressed members. Not providing shear reinforcement will make web shear cracks uncontrolled and equilibrium conditions will not be obtained.

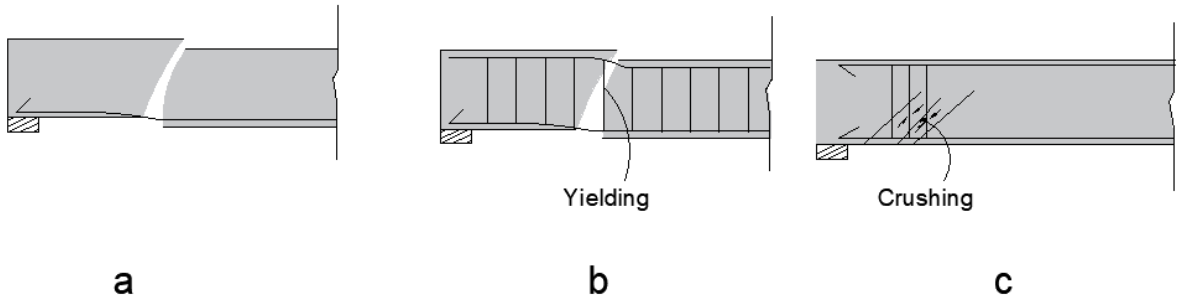

Figure 2.9 *Types of shear failure in a reinforced concrete member a) shear siding failure in a member without shear reinforcement b) shear sliding failure after yielding of shear reinforcement c) crushing concrete due to web shear compression failure. Based on Engström (2011b).*

2.4.3 Design for shear

2.4.3.1 Load Effect

The design shear force that should be resisted by the web, $V_{Ed,net}$, is given by:

$$V_{Ed,net} = V_{Ed} - V_{ccd} - V_{td} \tag{2.36}$$

V_{Ed} Total shear force from transverse load (Load effect), design value.

V_{ccd} Transverse component (design value) of the compressive resultant.

V_{td} Transverse component (design value) of the tensile resultant.

Prestressing delays cracking in a prestressed member and the prestressing force can be treated in two ways when acting on a structural member, Engström (2011). The first way is to consider the prestressing as an external load acting on the member and the second way is to consider it as an internal restraint. Based on Eurocode, the effect of prestressing force should be taken into account differently depending on if it is treated as an external load or as an internal restraint, already when the load effect is determined as stated in Equation (2.37). If the prestressing is treated as an external load, the transverse component of the prestressing force will influence the load effect. However, if prestress is treated as an internal restraint, the transverse component of the inclined prestressing force is accounted for as a reduction of the design shear force, similarly as for inclined compression and tensile chords.

$$V_{Ed,net} = V_{Ed} - V_{ipd} \quad (2.37)$$

V_{Ed} Design shear force (load effect).

V_{ipd} Transverse component (design value) of inclined prestressing force.

$$V_{ipd} = P_d * tan\alpha_p \quad (2.38)$$

The prestressing force has a design value that can be determined is as stated in formula below.

$$P_d = \gamma_p * P_{0\infty} = \gamma_p * \sigma_{P0\infty} * A_p \quad (2.39)$$

$\sigma_{P0\infty}$ Prestress in prestressing steel after long time.

A_p Total cross-section areas.

The approach to design concrete structures with regard to shear, in order to resist shear forces and bending moment, is based on the failures described in section 2.4.2. The shear design is made in ULS based on Eurocode (SIS, 2002a) and the structure is assumed to be cracked. Engström (2011) summarizes the appropriate following steps to design the shear in section for a prestressed member:

- Determine the shear forces that the web should be able to resist from the load effects, $V_{Ed,net}$.
- Determine the shear capacity, $V_{Rd,c}$, of the concrete section without shear reinforcement, and compare to the shear effect from the loads $V_{Ed,net}$. If $V_{Rd,c}$ is sufficient, minimum shear reinforcement should still be provided. If $V_{Rd,c}$ is insufficient, design of the shear reinforcement should be performed.

2.4.3.2 Members without shear reinforcement

The shear resistance for concrete members without shear reinforcement is governed by shear sliding failure along a flexural shear crack or a web shear crack. In members without shear reinforcement, shear resistance, $V_{Rd,c}$, is expressed by the Equation (2.40). It consists of two parts, the first one is based on friction and interlocking, and other part is based on arch action due to prestressing, Eurocode (SIS, 2002a).

$$V_{Rd,c} = \left(C_{Rd,c} * K * (100 * \rho_1 * f_{ck})^{\frac{1}{3}} + K_1 * \sigma_{cp}\right) b_w * d \quad (2.40)$$

$$V_{Rd,cmin} = \left(v_{min} + K_1 * \sigma_{cp}\right) * b_w * d \quad (2.41)$$

$$K = 1 + \sqrt{\frac{200}{d}} < 2, with\ d\ in\ mm \quad (2.42)$$

$$\rho_1 = \frac{A_{sI}}{b_w * d} \leq 0.02 \quad (2.43)$$

V_{Ed} Transverse shear force.

A_{sI} Statically required tensile area of reinforcement.

b_w Smallest width of cross section in tensile area

$$\sigma_{cp} = \frac{N_{ed}}{A_c} \quad (2.44)$$

N_{ed} Axial force in the cross-section due to loading or prestressing.

A_c Area of concrete cross section.

v_{min} National parameter recommended value is expressed in Equation (2.45).

$$v_{min} = 0.035 * K^{\frac{3}{2}} * f_{ck}{}^{\frac{1}{2}} \quad (2.45)$$

2.4.3.3 Members with shear reinforcement

In Eurocode (SIS, 2005a), the shear resistance for concrete members with shear reinforcement can be explained by a truss model. Figure 2.9 illustrates the truss model and shows the inclination of the cracks and struts, and the equilibrium condition that is affected by the strut inclination. Figure 2.10 shows the case of 45º inclination with the corresponding value 0.9d including the following notations:

V_{Ed} Total shear force from transverse load (Load effect).

F_s Resultant steel force.

F_c Resultant concrete force.

M_{Ed} Design value of the applied internal bending moment.

F_{sv} Vertical resultant steel force.

F_{cw} Inclined resultant concrete force.

σ_{cw} Inclined resultant concrete stress.

d Effective height depth.

R Reaction force in the support.

The recommended values of the strut inclination angle for reinforced members according to Eurocode (SIS, 2005a) are between 22º and 45º. The design of the shear reinforcement and the estimation of shear resistance is based on the truss model. This means that the contribution from friction and aggregate interlock to the shear resistance is disregarded.

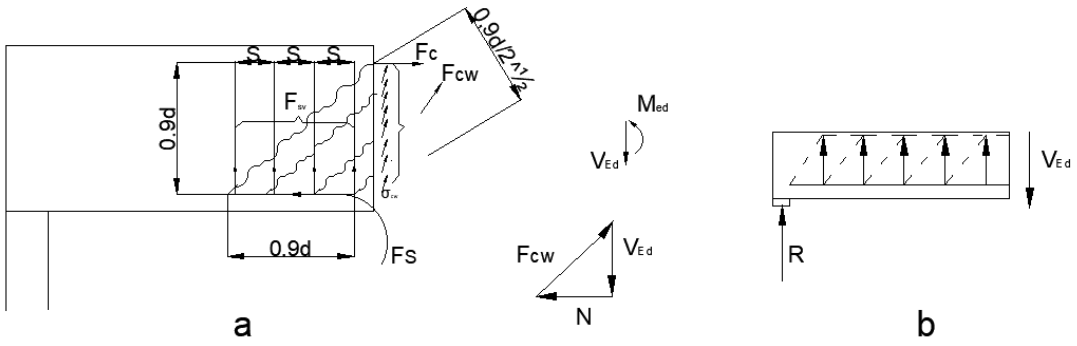

Figure 2.10 Equilibrium of a concrete member with shear reinforcement and inclined cracks a) equilibrium conditions b) Truss model with inclined struts and vertical ties. Based on Engström (2011b).

Longitudinal reinforcement is required to resist the longitudinal tensile force in the tensile chord. Figure 2.11 illustrates the truss model used for design of shear reinforcement. In the model, both the struts and shear reinforcement can have varying

angles. The model also put requirements on the amount of longitudinal reinforcement in the tensile chord. In Figure 2.11 the following symbols are shown:

α Angle between the shear reinforcement and the beam axis perpendicular to shear forces.

θ Angle between the concrete compression strut and the beam axis perpendicular to the shear forces. The recommended angle value varies based on type of concrete structures for reinforced structures the angle should be limited according to formula (2.46) whereas the limitation for the angle in prestressed structures is limited according to formula (2.47).

$$1 \leq \cot\theta \leq 2.5 \quad (2.46)$$

$$1 \leq \cot\theta \leq 3 \quad (2.47)$$

F_{td} is the design value of tensile force in the longitudinal reinforcement.

F_{cd} is the design value of tensile force in the longitudinal reinforcement.

b_w is the minimum width between tension and compression chord.

Z is the inner lever arm for a member, and the approximate value is $0.9d$.

d is the effective depth of the member.

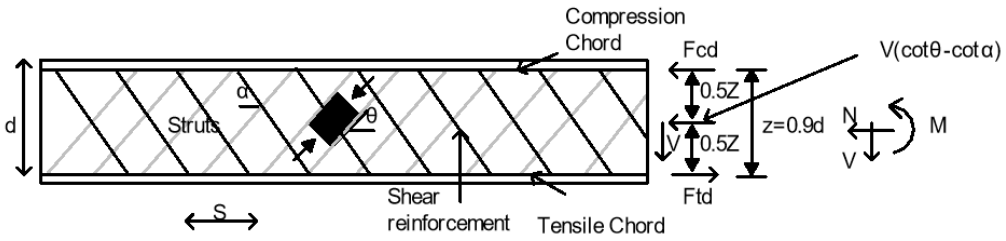

Figure 2.11 Shear reinforced members with relevant components according to Eurocode (SIS, 2005a).

Shear resistance against shear sliding failure for members with vertical shear reinforcement can be calculated as expressed in Equation (2.48), Engström (2011).

$$V_{Rd,s} = \frac{A_{sw}}{s} * Z * f_{ywd} \cot\theta \quad (2.48)$$

The upper limit of the shear resistance against the web shear compression failure for members with vertical shear reinforcement can be calculated as expressed in Equation (2.49), Engström (2011).

$$V_{Rd,max} = \alpha_{cw} * b_w * Z * V_1 * f_{cd}/(\cot\theta + \tan\theta) \quad (2.49)$$

The shear resistance for members with vertical shear reinforcement, is the minimum of Equations: (2.48) and (2.49).

A_{sw} Cross sectional area of shear reinforcement unit.

s Spacing of shear reinforcement.

f_{ywd} Design yield strength of shear reinforcement.

V_1 Strength reduction factor for concrete cracked in shear.

α_{cw} Coefficient considering of the state of stress in compression.

The maximum effective cross-sectional area of the shear reinforcement is limited according to Equation (2.50).

$$\frac{A_{sw,max}}{S*b_w} \leq 0.5 * \alpha_{cw} * V_1 * f_{cd} \quad (2.50)$$

If the shear reinforcement is inclined, the shear resistance is instead the minimum of the following Equations:

$$V_{Rd,s} = \frac{A_{sw}}{S} * Z * f_{ywd} \, (\cot\theta + \cot\alpha) * \sin\alpha \quad (2.51)$$

$$V_{Rd,max} = \frac{\alpha_{cw} * b_w * Z * V_1 * f_{cd} * (\cot\theta + \tan\theta)}{(1 + \cot^2\theta)} \quad (2.52)$$

Here, the maximum effective cross-sectional area of the inclined shear reinforcement is limited by:

$$\frac{A_{sw,max}}{S*b_w} \leq \frac{0.5*\alpha_{cw}*V_1*f_{cd}}{\sin\theta} \quad (2.53)$$

Stirrups, bent-up bars, cages and ladders are used as shear reinforcement. The most common type is stirrups, shown in Figure 2.12. The stirrups enclose the longitudinal and compression reinforcement in the upper and lower side of the cross section and extends into the compression zone.

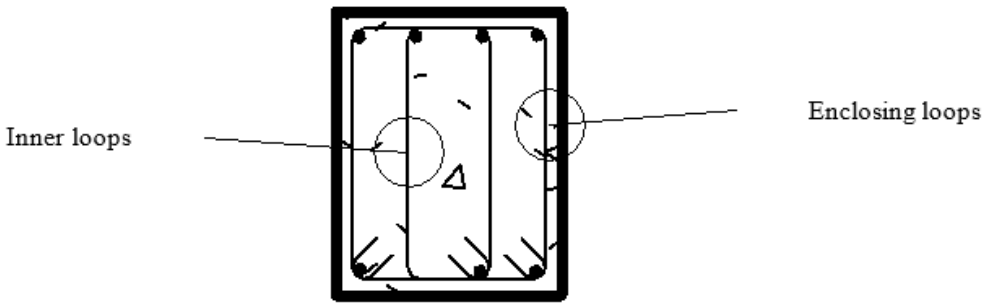

Figure 2.12 Stirrup reinforcement according to Eurocode (SIS, 2005a).

2.4.3.4 Minimum shear reinforcement requirements

If shear reinforcement is not needed, a certain amount of minimum shear reinforcement must be provided, Engström (2011). Engström (2011) specifies the minimum ratio of shear reinforcement that gives the minimum amount of the shear reinforcement expressed by Equation (2.54).

$$\rho_{w,min} = 0.08 * \frac{\sqrt{f_{ck}}}{f_{yk}} \quad (2.54)$$

f_{ck} Characteristic compressive cylinder strength of concrete at 28 days

f_{yk} Yield strength of reinforcement

And for yield strength $f_{yk} = 500MPa$ the shear reinforcement ratio is defined as stated in Equation (2.56).

$$\rho_{w,min} = \frac{A_{sw}}{S * b_w * \sin\alpha} \quad (2.55)$$

A_{sw} Cross sectional area of shear reinforcement.

S Spacing of the shear reinforcement units along longitudinal axis.

Transportstyrelsen (2018) have similar requirement for the minimum ratio of shear reinforcement which is stated in Equation (2.56)

$$\rho_{w,min} = (0.1 + 0.05\frac{h}{b_w}) \quad (2.56)$$

h Height of the concrete section

b_w Effective width of concrete section.

Determination of minimum ratio shear reinforcement is expresses by Equation (2.57).

$$\rho_{w,min} = \max(\frac{A_{sw}}{S * b_w * \sin\alpha}, 0.1 + 0.05\frac{h}{b_w}) \quad (2.57)$$

The final minimum area of the shear reinforcement is expressed by formula (2.58)

$$A_{smin} = \rho_{w,min} * b \quad (2.58)$$

b Width of concrete section.

2.5 Torsion

According to Eurocode 2. Torsional moments and are calculated separately and combined in order to design total shear and torsional reinforcement. The torsion is resisted by shear stress forming a closed shear flow around the cross-section. For each edge of the cross-section, the shear stresses caused by the torsional moment and the shear force can be added together, and the transversal reinforcement in each edge designed for the sum, see Figure 2.13. The strut inclination is influenced by the torsion, and the strut will become less steep on the side where the shear stresses interact and steeper where on the side where they counteract each other.

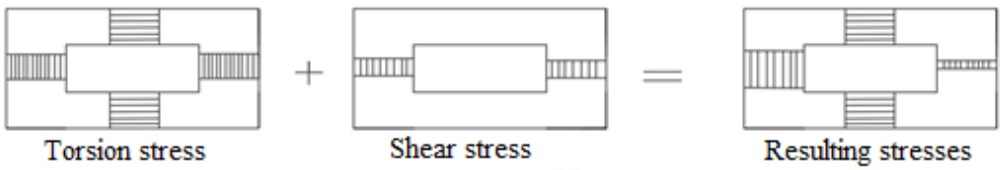

Figure 2.13 Combination of the shear forces and torsional stresses according to Eurocode (SIS, 2005a).

Pure torsional moment can be calculated as stated in Equation (2.59).

$$\tau_{t,i} * t_{ef,i} = \frac{T_{ed}}{A_k} \quad (2.59)$$

Shear force in a wall due to torsion is given by Equation (2.60).

$$\tau_{t,i} * t_{ef,i} * z_i = V_{Ed,i} \quad (2.60)$$

T_{ed} Applied design torsion. See Figure 2.14.

A_k Area enclosed by the center lines of the connection walls, including inner hollow areas.

z_i Side length of the wall.

$\tau_{t,i}$ Torsional shear stress in wall.

t_{eif} Effective wall thickness can be calculated according to Equation (2.61).

$$t_{eif} = \frac{A}{u} \tag{2.61}$$

A Total cross section area.

u Outer circumference of the cross section.

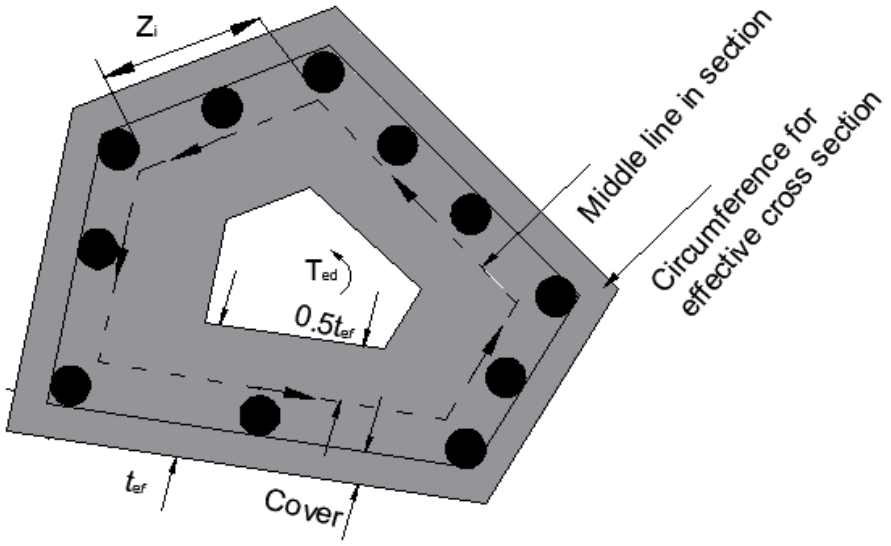

Figure 2.14 Torsion in concrete section according to Eurocode (SIS, 2005a).

The required area for longitudinal torsion reinforcement can be calculated as stated in Equation (2.64)

$$\frac{\sum A_{sl} * f_{yd}}{u_d} = \frac{T_{ed}}{2A_k} * \cot\Theta \tag{2.64}$$

u_k Perimeter of the area A_k.

f_{yd} Design yield stress of the longitudinal reinforcement.

Θ Angle of the compression strut.

Only minimum reinforcement in the cross section is needed if Equation (2.65) is fulfilled.

$$\frac{T_{Ed}}{T_{Rd.c}} + \frac{V_{Ed}}{V_{RD.c}} \leq 1 \tag{2.65}$$

T_{Ed} Design torsional moment

V_{ED} Design transverse force

$T_{Rd,c}$ Design torsional cracking moment

The load bearing capacity at torsion and shear force is limited by the capacity of the concrete compressive strut according to the Equation (2.66).

$$\frac{T_{Ed}}{T_{Rd.max}} + \frac{V_{Ed}}{V_{RD,max}} \leq 1 \quad (2.66)$$

T_{Ed} Design torsional moment

V_{ED} Design transverse force

$T_{Rd,max}$ Design torsional resistance moment.

2.6 Cost and global warming potential

The two evaluation criteria used in this study are environmental impact and investment cost. As mentioned in Section 1.4, they are evaluated by global warming potential (GWP) and Swedish crowns (SEK). Both criteria depend on the production method used and the material class of the concrete and reinforcement steel. Since this thesis is based on Aspegren & Möörk (2021) the same procedure and basic values are used. For instance, the way to evaluate the GWP is to sum the effect of greenhouse emissions in CO2-eq. This way, it is possible to compare the effect of different greenhouse gases and their impact on global warming.

Assumptions and values made by Aspegren & Möörk (2021) that are used in this study as well are:

- CO2-eq are calculated per cubic meter material.
- The concrete class is C35/45 shown in table 2.4.
- Investment cost only includes the superstructure of the bridge. The total cost of the bridge is not calculated.

From an economic aspect, every bridge alternative will be evaluated by calculating the cost of concrete and reinforcement steel separately. The amount of work is included by multiplying time of work by the hourly cost of one construction worker. Then the final cost is calculated and presented for each bridge. The state standard cost and time values for bridges in the construction stage in Sweden, used in this study, are shown in Table 2.4.

Table 2.4 Material and work costs for prestressing steel. From Aspegren & Möörk (2021).

	Material cost	**Work time**	**Work cost (500 SEK/h)**
Anchor	5000 SEK	3h	1500 SEK
Cable / Duct	450 SEK/m	0.15 h/m	75 SEK/m
Non-prestressed reinforcement (total cost)	20000 SEK/m^3		

The values for GWP and cost that are applied to evaluate the bridge design alternatives are presented in Table 2.5.

Table 2.5 materials' cost and CO2- eq. From Aspegren & Möörk (2021).

	GWP [CO_2-eq/m^3]	Cost [SEK/m^3]
Concrete C35/45	388	1800
Prestressing steel	8580	*
Non-prestressed steel	5148	*

* Values are mentioned in Table2.4

3 Parametric optimization

In this chapter the theory of optimization in parametric design in an early stage of design process is highlighted. According to Gosavi (2015) simulation-based optimization is a method that uses computers to analyze random systems by generating numerous solutions. Overall, optimization techniques can be divided into two main branches; parametric (static) optimization and controlled (dynamic) optimization. In parametric optimization, which will be the method used in this thesis, a set of parameters are combined to measure a specific performance, e.g. through a structural analysis, in order to reduce cost or optimize performance.

3.1 Parametric modelling

In construction sector, parametric modelling is mainly developed for buildings but has recently been increasingly used for infrastructure projects, according to Girardet & Boton (2021). The authors explain that this method has confirmed its effectiveness in reducing costs and its ability to be reused in different types of projects. Fu (2018) explains that in a parametric design process of complex concrete structures, parametric modelling can be implemented using a programming code or a script to set up geometries, loads, boundary conditions and reinforcement layout. The main benefit with parametric modelling is that once the 3D model is set, it is easy to change any of the parameters without needing to rebuild the model, instead the model is built automatically. This facilitates involving different stakeholders early in the process, making it handy to manage iterations to obtain the desired solution.

3.2 Parametric design

In the context of automating the construction industry and the efforts to achieve better collaboration between design and construction stages, attempts are made to combine set-based design (SBD) and parametric design methods with finite element and multi-criteria decision analyses (Rempling, et al., 2019). This is to replace the traditional point-based design (PBD) where decision making is a gradual process based on one criterion at a time. Common multi-criteria in bridge projects can be represented by choices such as the materials used, that need to fulfill cost and environmental requirements, as well as the type and the structural system of the bridge. Rempling, et al. (2019) refers to recent research that explores the possibility to further implement SBD in prestressed concrete road bridges and to estimate reinforcement.

Set-based parametric design (SBPD) is a further development of SBD which integrates parametric modelling with SBD (Rempling, et al., 2019). Sets of design choices are considered thoroughly and evaluated in relation to various criteria to eliminate inefficient solutions. For example, cost and environmental impact can in early stages be integrated with structural design process to reach the most efficient design solution. For this thesis SBPD is applied to optimize concrete and reinforcement quantities for a continuous post-tensioned concrete bridge according to the criteria mentioned.

Aspegren & Möörk (2021) presented the workflow of designing a prestressed concrete bridge. Figure 3.1 shows the complexity of the design compared to a normal reinforced

bridge. In a prestressed concrete bridge, the tendon layout, its eccentricity, and the geometry of the structure are decisive for the obtained shear forces and torsional moments. The notation in the workflow is as follows:

M_s Secondary moment.
M_{Ed} Design moment.
M_{Rd} Moment capacity.

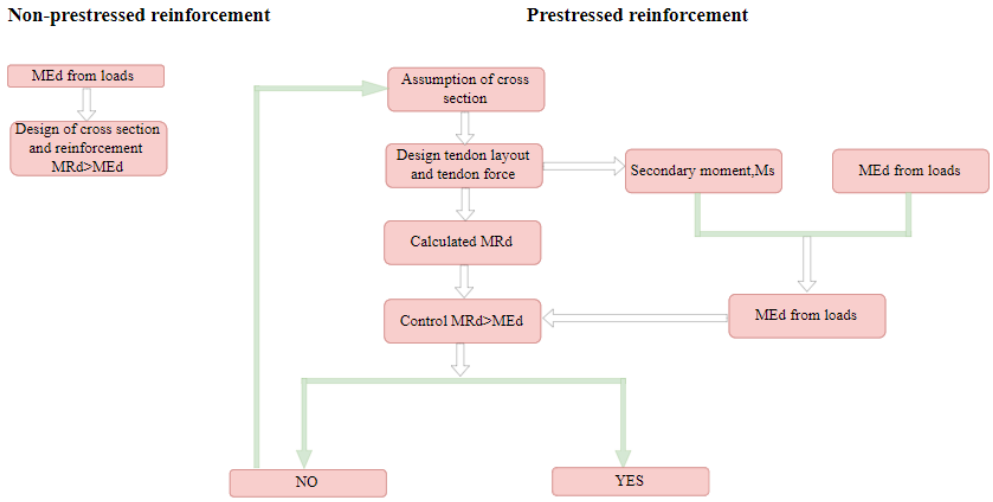

Figure 3.1 *A comparison of the design process for a normal reinforced concrete bridge and a prestressed concrete bridge. From (Aspegren & Möörk, 2021).*

Limitations in design approaches nowadays can be demonstrated by the traditional two-dimensional (2D) computational aided design. Using a parametric design method, such as SBPD, combined with an optimization tool gives the opportunity to generate 3D models allowing to implement changes in the preliminary phase of design process (Girardet & Boton, 2021). In this thesis, the optimization tool will be a python script where the different types of non-prestressed reinforcement are optimized.

4 Parametric modelling for prestressed bridge

This chapter briefly describes the FE model built by Aspegren & Möörk (2021), the elements used for the structural parts, the material choices and how these influence the structural behavior of the bridge. The loads acting on the bridge and how they are applied, as well as load combinations extracted from the python script and used in the design of reinforcement are described as well. Furthermore, the theoretical assumptions that have been made and the modifications made on the python script to obtain essential output data are presented.

4.1 Finite element model

The FE model used in this thesis was originally developed by Aspegren & Möörk (2021) and consists of beam elements to represent the main bridge girder. It is defined by the geometries of the structural elements and the tendon layout, including the boundary conditions and connections between them and the structural elements. Verifications for both the mesh size and the FE results have been made by a convergence study and by comparing to hand calculations, respectively.

The wingwalls are ordered longitudinally of the bridge, wingwalls consist of length of wingwall L_{ww} and the two heights the first height is the height of the end of wingwalls H_2, and the other height of the wingwalls H_1, the closest height to the bridge. Moreover, the slope with value 1:2 between two heights for the wingwalls. The height of the end-shields is equal to H_1, the L_{ww} is 5.8m and $H_2$is 1.1m as modelled by Aspegren & Möörk (2021)

The tendon layout has been integrated to the FE model with a built-in spline tool in BRIGADE/Plus developed by Aspegren & Möörk (2021). 6 points have been defined in the tool in order to control the parabolic tendon layout. The points represent coordinates that can be adjusted through testing different values and thereby determine the tendon layout, see Figure 4.1. When determining the tendon layout two important parameters have been identified i.e., the distance where the bending moment is zero L_0 and the eccentricity e_{span}. L_0 extends from point 2 to point 5. The eccentricity extends to the lowest point the tendon reaches in the span, e_{span}. The e_{span} is depended on factor α_{span} that has recommended values between 0% and 20% by the experience structural engineer.

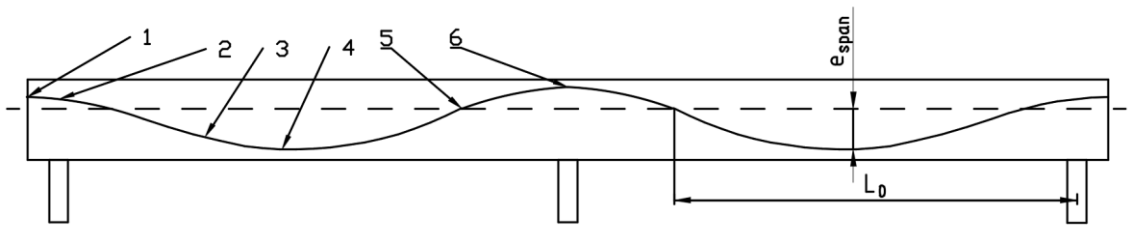

Figure 4.1 Entered values to model tendon layout. Based on Aspegren & Möörk 2021.

The geometries of the structural parts are chosen to represent a common bridge of the bridge type studied, consisting of the main beam and bridge deck as well as two cross beams, end-shields and wingwalls at the end supports. The base FE model has parametrized geometry that can be changed depending on the case specific input. For

instance, the bridge span and width, and the main beam dimensions can be changed to represent the bridge studied.

The main beam is an important structural part of the bridge, transferring the main loads to the cross beams and further on to the supports. The main beam's cross-section is a T-section that has a constant dimension along the bridge spans. The element type that was used to model the main beam is beam elements. The sectional forces, stresses, shear forces and bending moment, are obtained from the main beam.

Over the main beam a shell element has been modelled to represent the bridge deck. The shell element functions as a loading area in which the traffic loads are applied. It was modelled with a fictious material carrying the loads only in transverse direction. In this way the traffic loads are directly transferred to the main beam. This is a common approach in bridge design used in engineering practice to focus the design on the main beam where all the sectional forces are obtained. For this reason, the bridge deck as well as the edge beams, end-shields and wingwalls have a load transferring function and their properties should not affect the main beam.

The cross beams were modelled with the same concrete class as the main beam. Their main function was to enable accurate load transfer to the supports and they give the possibility to include the substructure in the FE analysis, if needed. Beam elements with a fictious material but including the self-weight have been used in modelling the edge beams.

4.2 Loads and load combinations in FE model

In this section both permanent and variable loads are described as well as their combinations and how they are used in obtaining the results. Only vertical loads are included in the FE model, since horizontal loads mainly affect the substructure which is out of the scope of this thesis.

4.2.1 Permanent loads

Permanent loads that were included in the FE model are the self-weight of the structural parts, included through their densities, as well as the earth pressure, support displacement and shrinkage. The earth pressure is applied on the end-shields and is calculated at rest as stated in Equation (4.1).

$$q_{earth.rest}(z) = K_0 * \gamma * z \tag{4.1}$$

$q_{earth.rest}(z)$	Earth pressure at rest depending on depth (z)
z	Depth from zero-pressure level
K_0	Earth pressure coefficient at rest
γ	Earth density

Support displacement is accounted for in the vertical direction only. The vertical support displacement was prescribed to 20 mm for each of the three supports. Shrinkage was accounted for through a temperature drop $T_{shrinkage}$ in the entire bridge which leads to shortening of the bridge, see Equation (4.2).

$$T_{shrinkage} = \frac{\varepsilon_{cs}}{\alpha_c} \quad (4.2)$$

ε_{cs} Shrinkage strain.

α_c Concrete theramal expansion coefficient.

4.2.2 Variable loads

Variable loads that were included in the FE model are temperature load, surcharge load and traffic loads. Braking load have been neglected since its effect is assumed to be minor on the superstructure. Temperature load has been included due to that its elongation causes increased earth pressure on the end-shields, see Equation (4.3).

$$q_{earth.increase} = \delta * 200 * (K_p - K_0) * \gamma \quad (4.3)$$

$q_{earth.increase}$ Increased earth pressure due to elongation.

δ Horizontal movement of the bridge on each side. Maximum $H_1/200$ [m].

H_1 Height of end-shield.

K_p Coefficient for passive earth pressure.

Similarly as temperature increase, surcaharge loading causes an increased earth pressure on the end-shields when a vechile is placed outside the bridge deck. Since only the superstrucutre is studied, double-sided surcharge loading is checked. Furthermore, to calculate the surcharge load, 6 meters of the bridge width is considered to have higher load than the remaing width. Both parts or strips of the bridge, with higher and lower loading, contribute to the surcharge load which in average will be as stated in Equation (4.4).

$$q_{earth.increase} = K_0 * \frac{6m*20*\frac{kN}{m^2}+(B_{es}-6m)*10\frac{kN}{m^2}}{B_{es}} \quad (4.4)$$

B_{es} Width of the end-shield.

4.2.3 Load combinations and groups

The module *load combinations* in BRIGADE/Plus has been used for the load combinations described in Sections 2.3.3 and 2.3.4. In this module, load groups are formed and different load cases are combined in ULS and SLS. From the load combinations, the sectional forces; shear force V, torsional force T and normal force N, were obtained from BRIGADE/Plus by adjusting the python script developed by Aspegren & Möörk (2021). The sectional forces are obtained for the maximum and minimum shear and torsional forces ($V_{\max}$, $V_{\min}$, $T_{\max}$, T_{min},), respectively. E.g., $V_{\max}$ has a maximum shear force V and associated torsional moment T and normal force N as Table 4.1 shows. $T_{\max}$ has a maximum torsional moment T and shear force V and normal force N. The normal force is the result of the prestressed tendons and varies along the bridge. The variable x is the sections along the bride where the sectional forces are extracted from FE analysis.

Table 4.1 Layout of a table with results from a load combination, showing sectional forces for the sections of the bridge.

	ULS											
	Vmax			Vmin			Tmax			Tmin		
x	V	T	N	V	T	N	V	T	N	V	T	N
m	kN	kNm	kN	kN	kNm	kN	kN	kNm	kN	kN	kNm	kN

4.3 Reinforcement arrangement

In this thesis optimization of the of the non-prestressed reinforcement includes four different types; stirrup reinforcement A_{sv1} and A_{sv2} , horizontal transversal reinforcement $A_{s.h}$ and horizontal longitudinal reinforcement $A_{s.l}$, all shown in Figure 4.2. These types of reinforcement form the shear and torsinal reinforcement in the bridge, The torsion reinforcement consist of three categories: $A_{s.h}$, $A_{s.l}$ and A_{sv1}. The vertical shear reinforcement A_{sv2} consists of two stirrups, as shown in Figure 4.2, each designed against half of the maximum of the shear forces presented in Table 4.1 for every section. The total amount of reinforcement A_{sv2} is calculated according to Equation (2.48). The stirrup enclosing the cross section of the web consists of A_{sv1} and $A_{s.h}$ and is designed against the maximum of the torsional moments presented in Table 4.1 for every section. The torsional moments are converted to shear forces according to Equation (2.60). The amount of reinforcement A_{sv1} is then calculated in the same way as A_{sv2} according to Equation (2.48) by providing the shear resistance V_{Rds} that corresponds to the converted shear forces. The total amount of stirrup reinforcement, A_{sv1} from torsion and A_{sv2} from shear, is summed up according to the principle presented in Figure 2.13.

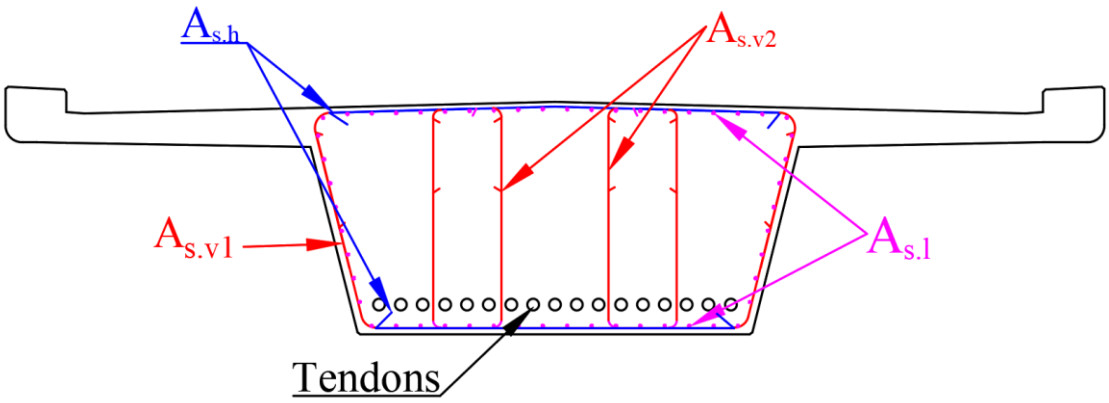

Figure 4.2 Reinforcement types in the span cross section of the bridge beam.

The horizontal torsional reinforcement $A_{s.h}$ consists of two horizontal rebars at the upper and lower edges of the cross section, respectively, as shown in Figure 4.2. The torsional moments are converted to shear forces according to Equation (2.60). The amount of reinforcement $A_{s.h}$ is then calculated according to Equation (2.48) by providing shear resistance V_{Rds} corresponding to the converted shear forces. The difference between vertical shear reinforcement A_{sv1} and horizontal torsional reinforcement $A_{s.h}$ comes from the difference in the direction of the inner lever arm. In Equations (2.48) and (2.60), the inner lever arm z_v of the reinforcement A_{sv1} is taken in the vertical direction while the inner lever arm z_h of the reinforcement $A_{s.h}$ is taken in the horizontal direction.

The last type of torsional reinforcement is the longitudinal reinforcement $A_{s.l}$ that extends in the plane of the bridge cross section. This reinforcement is designed against the maximum applied design torsional moments from Tmax and Tmin according to Equation (2.62).

4.4 Input data for optimization

The input data for the optimization in this study was the same as in the work by Aspegren & Möörk (2021), and is presented in Table 4.2. The case-specific input data for different results studied are presented in separate tables in each section.

Table 4.2 General input data for results presented. Based on Aspegren & Möörk and complemented with properties of non-prestressed reinforcement.

Bridge	
Span length [m]	*
Width [m]	*
Cross section	
Thickness top flange t_f [m]	0.3
Web width [m]	Width/2
$CCduct$ [m]	0.25
Wing walls and end shields	
Length of wing walls, L_{ww} [m]	5.8
H_2 [m]	1.1
Edge beam	
Width [m]	0.5
Height[m]	0.5
Materials	
Concrete class	C35/45
Prestressing steel f_{bk} [MPa]	1860
Non-prestressed reinforcement	**
f_{yd} for vertical reinforcement [MPa]	300
f_{yd} for longitudinal and horizontal reinforcement [MPa]	435
f_{yd} Tensile strength [MPa]	1860
Steel density [kg/m3]	7800
Diameter [mm]	16

* Depending on each specific case.
** Determined with respect to shear and torsion.

The mesh size is a decisive factor for the computational time that is needed to run the FE analysis. Due to the limitation in time in this thesis, all FE analysis could not be run with the finer mesh $L/100$. Instead, the mesh size $L/50$ is used in sections 6.1 – 6.2 and $L/100$ is used in section 6.3 to run one existing bridge. Since a mesh study is not performed in this thesis, the error marginals presented by Aspegren & Möörk (2021) are accepted.

5 Optimization with set-based parametric design

The set based parametric design is the method used to accomplish the optimization. The parameters used in the optimization are the beam height, h, the number of tendons, n_{tendon}, the distance between end support and the point where the tendon meets the center of gravity of the beam, L_0, the maximum eccentricity of the tendon in the span, e_{span}, and the inclination of compressive struts, θ. The loads, dimensions, load combinations, and parameter combinations are defined by the python script. The analyses of finite elements are performed by BRIGADE/Plus (Scanscot Technology, 2021). The model can automatically be updated by changing values of input parameters and their sets. Moreover, the most favorable optimization for shear and torsion reinforcement design is chosen to achieve the most beneficial design.

5.1 Optimization of beam height

The relation between non-prestressed reinforcement and beam height is studied in the optimization, since there are no guidelines that determines the optimal relation between them. The optimization is performed by comparing different beam heights with the corresponding reinforcement quantities with regard to cost and GWP.

5.2 Reinforcement optimization for shear and torsion

The amount of shear and torsion reinforcement depends on the beam height. As explained in section 4.3, the amount of shear and torsion reinforcement is designed for the maximum of the shear forces and torsional moments shown in Table 4.1. The shear forces and torsional moments calculated by BRIGADE/Plus are compared with shear and torsional resistance, respectively, as stated in Equations (5.1) and (5.2)

$$V_{Rdc} \geq V_{Ed} \tag{5.1}$$

$$T_{Rdc} \geq T_{Ed} \tag{5.2}$$

In order to determine if minimum reinforcement is enough, the interaction between concrete shear and torsion capacities is checked, as stated in Equation (2.65), otherwise shear and torsion reinforcement is required. When shear and torsional reinforcement is needed the inclined concrete compressive struts are checked according to Equation (2.66). The optimization method is based on testing different inclination angles θ between 18.4° and 45°; these values are recommended by experienced engineer in order to obtain the most optimized amount of shear and torsion reinforcement. The values of inclination angles have been changed with an increment of 0.1 in the interval stated in Equation (2.47). This increment has been chosen in order to take into account small changes in angles inclination to calculate corresponding reinforcement quantities accurately. For every angle, all reinforcement categories are summed up. Finally, the angle that gives the minimum amount of reinforcement gives the most optimal solution. The design approach including the optimization is illustrated in Figure 5.2.

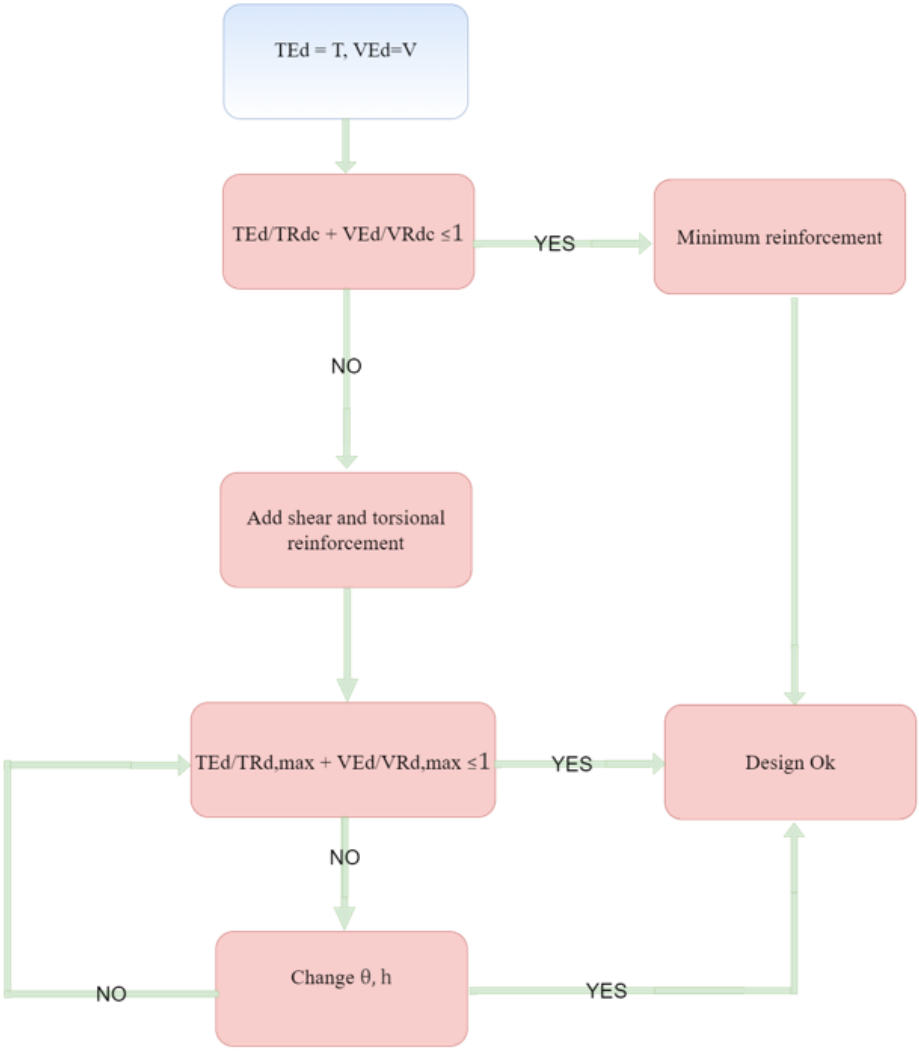

Figure 5.1 *Procedure of the optimization approach and the design checks for shear and torsion non-prestressed reinforcement.*

5.3 Optimization summary

In this thesis, the optimization of non-prestressed reinforcement has been performed as described in Section 5.2, for the optimized tendon layout and number of tendons determined by Aspegren & Möörk (2021). The optimized tendon layout was determined with respect to that the secondary moment varies depending on to the parameters e_{span} and L_0. Figure 5.2 shows the optimization summary where the inclination angle θ is added to the final optimization procedure. The same previous figures show the optimization sets to be used in sections 6.1 – 6.4. In section 6.1, the set e_{span} has three values and the set L_0 has two values. In section 6.2 – 6.4, the sets e_{span} and L_0 have one value each to save computational time. Values of e_{span} and L_0 are based on to Aspegren & Möörk (2021) assumptions. The set of e_{span} is based on

α_{span} which includes the values 0%, 10% and 20% while the set of L_0 includes the parameters 75% and 85%. The set of h is determined by the designer and only the beam heights that fulfill the design checks are included in the results. Finally, the set of inclination of compressive struts θ is between 18.4˚ and 45˚

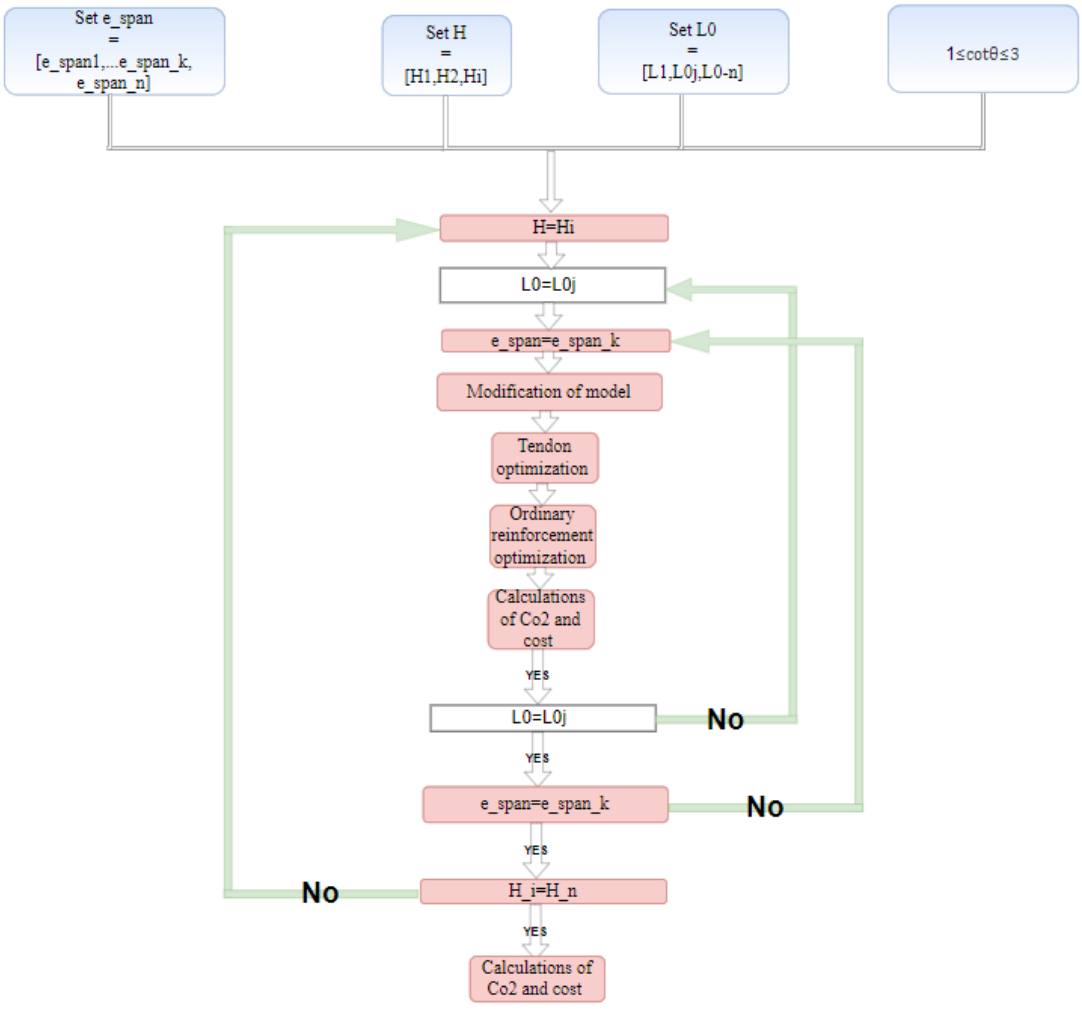

Figure 5.2 Procedure of the optimization approach.

6 Results

The results obtained from the optimization performed are presented in this chapter. The relations between beam height and reinforcement quantities, between span length and reinforcement quantities, and the relation between an existing bridge and an optimized bridge with respect to GWP and cost is studied. This was made in order to better understand the optimal relation between beam height, span lengths and quantities of non-prestressed reinforcement.

6.1 Relation between beam height and quantities of reinforcement

The relation between beam height and the amount of reinforcement needed was studied for two bridge geometries, presented in Table 6.2. The same two bridge geometries were also studied by Aspegren & Möörk (2021).The purpose of choosing these specific geometries was to include a bridge with a small width and span length and a bridge with larger width and span length. By including different dimensions and geometries, the relation between non-prestressed reinforcement and beam height can be better understood. The optimized non-prestressed reinforcement quantities for bridge 1 and 2 were 0.79 and 1.6 m^2/m, respectively.

Table 6.1 Bridges used for relation between beam height and the amount of non-prestressed reinforcement.

	Bridge 1	**Bridge 2**
Span lengths [m]	30	34
Width [m]	8	11
Web width [m]	4	5.5
Corresponding number of tendons	20	22
Reinforcement [m^2/m]	0.79	1.6

Figure 6.1 shows the optimized amount of reinforcement for different beam heights in the set h. The intervals of the set of beam heights h, was 100 mm in the interval 1.3 to 2.3 m. The solutions are approved with regard to both the number of tendons and the reinforcement design checks.

Figure 6.2 displays the total cost of bridges 1 and 2 for the optimized solutions in Figure 6.1. Corresponding inclination of compressive struts and number of tendons are shown in Table 6.2.

Figure 6.3 displays the GWP of bridges 1 and 2, including both reinforcement and concrete quantities, for the optimized solutions in Figure 6.1.

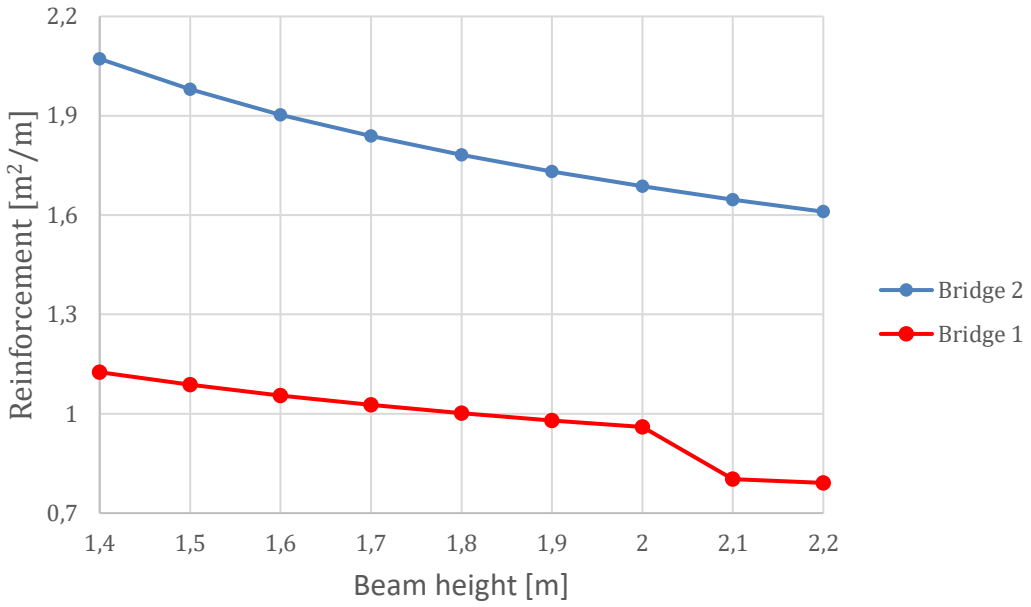

Figure 6.1 *Optimized quantities of non-prestressed reinforcement for different beam heights, for the two bridge geometries studied.*

Table 6.2 *Optimized quantities of non-prestressed reinforcement for different beam heights, with corresponding inclination of compressive strutsand number of prestressing tendons.*

	Beam height [m]	**Non-prestressed reinforcement [m²/m]**	**Inclination of compressive struts θ [degree]**	**No.of tendons**
Width 8m	1.4	1.126	37.57	20
	1.5	1.088	37.57	20
	1.6	1.055	37.57	20
	1.7	1.027	37.57	20
	1.8	1.001	37.57	20
	1.9	0.980	37.57	20
	2.0	0.960	37.57	20
	2.1	0.802	45	20
	2.2	0.791	45	20
Width 11m	1.4	2.072	37.57	22
	1.5	1.980	37.57	22
	1.6	1.903	37.57	22
	1.7	1.839	37.57	22
	1.8	1.782	37.57	22
	1.9	1.732	37.57	22
	2.0	1.687	37.57	22
	2.1	1.647	37.57	22
	2.2	1.611	37.57	22

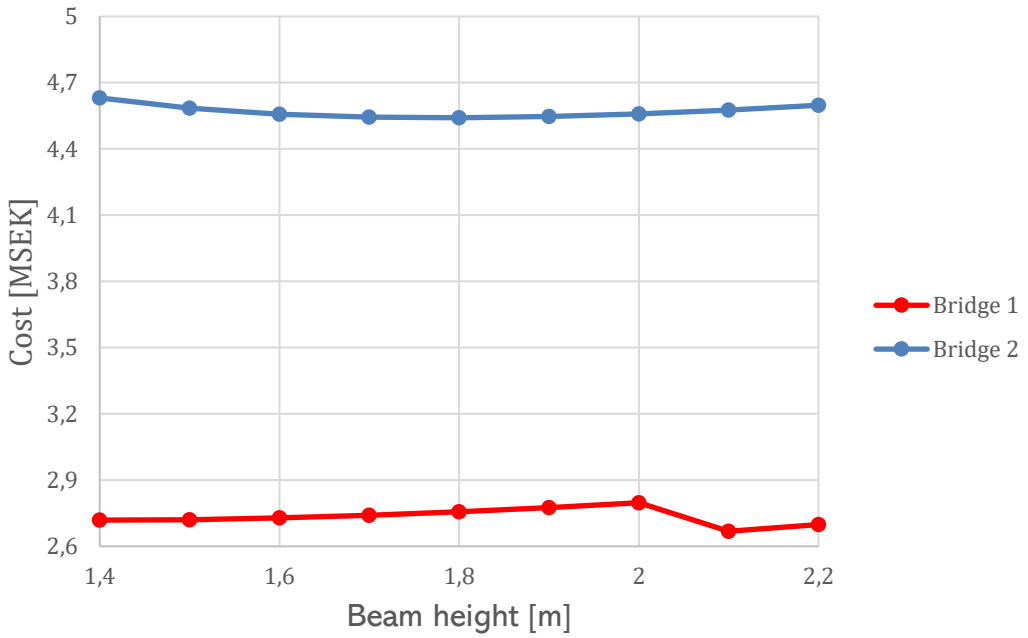

Figure 6.2 *Cost for different beam heights, with optimized quantities of non-prestressed reinforcement.*

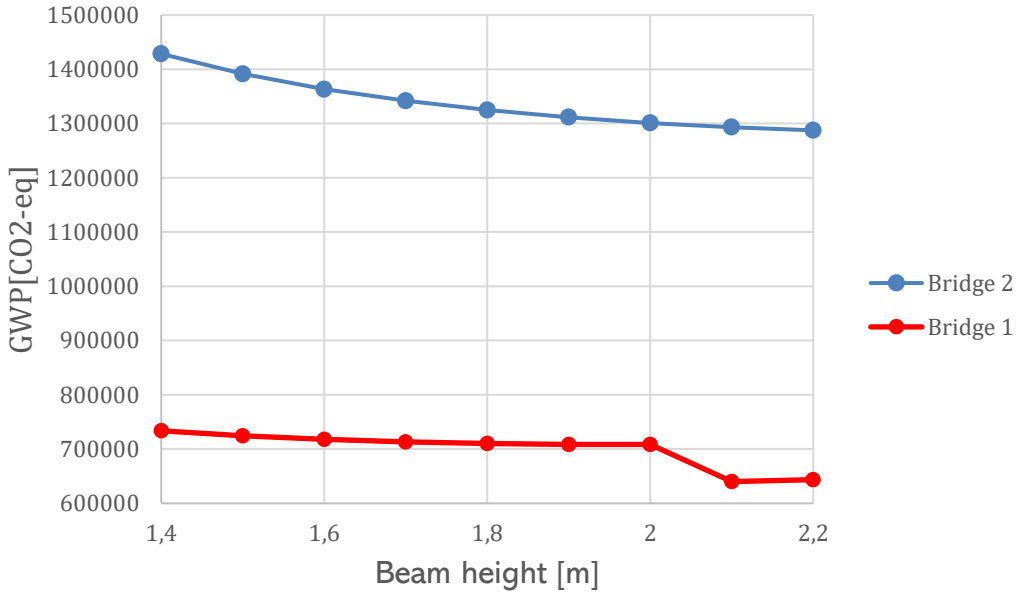

Figure 6.3 *GWP for different beam heights, with optimized quantities of non-prestressed reinforcement.*

6.2 Reinforcement quantities for different span lengths

Two bridges with the same widths as in Section 6.1, Table 6.2, are studied by modifying their length from 28 m to 36 m. The set *h* will contain the varying of the beam height from 1.3 to 2.2 with interval 100 mm, based on recommendations from experienced structural engineers. All beam heights which cannot fulfill the design demands are

excluded from the results. Figure 6.4 presents the optimized amount of reinforcement for different span lengths for bridges that fulfills the design checks. Table 6.3 shows reinforcement quantities together with the corresponding inclination of compressive struts, α_{span}, number of tendons. L_0 have been set to a constants fraction of the span length to keep the computational time low. The table shows how the amount of reinforcement per meter bridge length is affected by the span length. The results also show the optimal inclination of compressive struts.

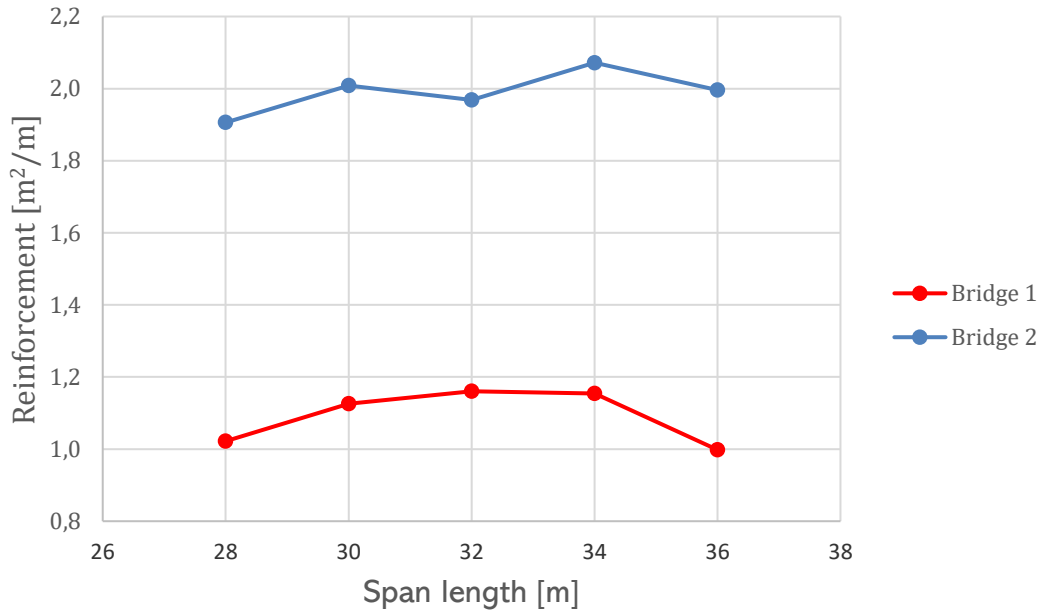

Figure 6.4 *Optimized quantities of non-prestressed reinforcementfor different span lengths.*

Table 6.3 *Optimized quantities of non-prestressed reinforcement for for different span lengths with minimum beam.*

	Span lengths	**Beam height[m]**	**Non-prestressed reinforcement [m²/m]**	**Inclination of compressive struts θ [degree]**	**α_{span}**	**tendons**	**L_0**
Width 8m	28m	1.6	1.02	37.57	20%	20	$0.75L_{span}$
	30m	1.4	1.13	37.57	20%	20	$0.75L_{span}$
	32m	1.4	1.16	37.57	20%	20	$0.85L_{span}$
	34m	1.5	1.15	37.57	10%	20	$0.85L_{span}$
	36m	1.5	1.00	45	10%	20	$0.85L_{span}$
Width 11m	28m	1.3	1.91	37.57	20%	22	$0.75L_{span}$
	30m	1.3	2.01	37.57	20%	22	$0.75L_{span}$
	32m	1.4	1.97	37.57	20%	22	$0.85L_{span}$
	34m	1.4	2.07	37.57	10%	22	$0.85L_{span}$
	36m	1.6	2.00	37.57	0%	22	$0.85L_{span}$

*$e_{span} = L_{CG} - (200\text{mm} + a_{span} * L_{CG})$

6.3 Comparison between optimized bridge design and existing bridge 100-411-1

In order to evaluate the results of the optimization method, an optimized bridge design is compared with the existing bridge 100-411-1, previously designed by Inhouse Tech Göteborg AB. Bridge 100-411-1 and the optimized bridge have the same width and span lengths. The input data is presented more in detailed in Table 6.4.

Table 6.4 Input data for the optimized bridge and the existing bridge 100-411-1.

Bridge	**Optimized Bridge**	**100-411-1**
Span lengths [m]	32	32
Bridge deck width [m]	11	11
Cross section		
Thickness top flange t_f[m]	0.30	0.29
Height H [m]	(1.3 - 2.3)	1.67
Web width b_w [m]	5.5	5.6
$CCduct$ [m]	0.19	0.25
Wing walls and end shields		
Length of wing walls[m]	5.8	5.8
H_2[m]	1.1	1.1
Edge Beam		
Width[m]	0.5	0.5
Height[m]	0.50	0.455
Materials		
Concrete class	$C35/45$	$C35/45$
Prestressing steel,f_{pk} [MPa]	1860	1860
Strand area [mm^2]	150	150
Number of strands per tendon [-]	15	15
Tendon layout		
$e_{span}[mm]$	710	710
L_0 [m]	27	27.0
Number of tendons	(0-27)	19

Figure 6.5 presents the amount of reinforcement for the existing bridge and optimized amounts of reinforcement for different beam heights for the optimized bridge that fulfills the design checks.

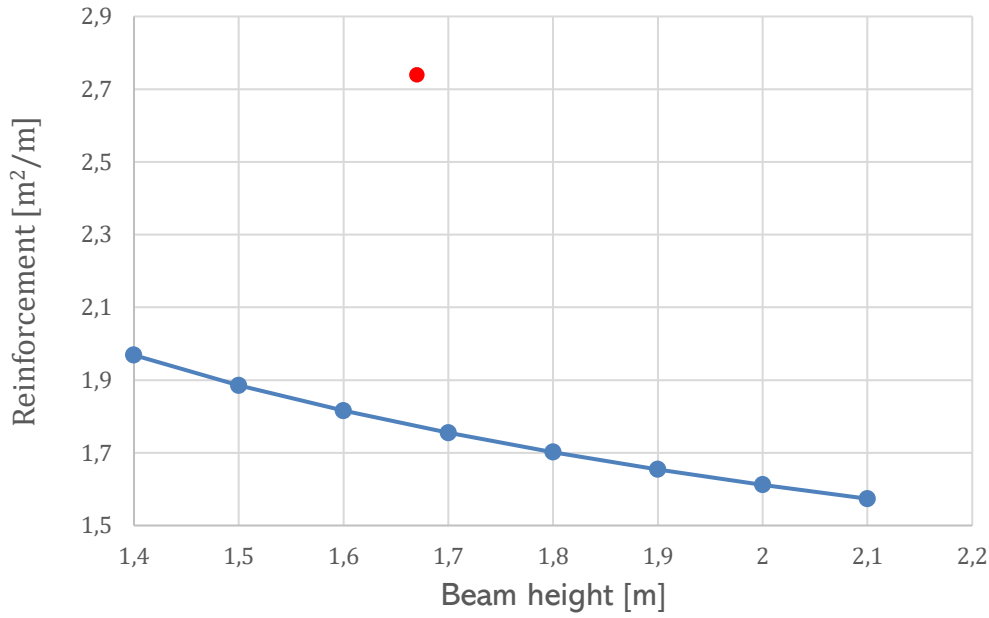

Figure 6.5 *Comparision of non-prestressed reinforcement quantities between the existing bridge and corresponding optimized bridge solutions.*

Figure 6.6 shows the cost of the existing and the optimized bridge solutions in Figure 6.5.

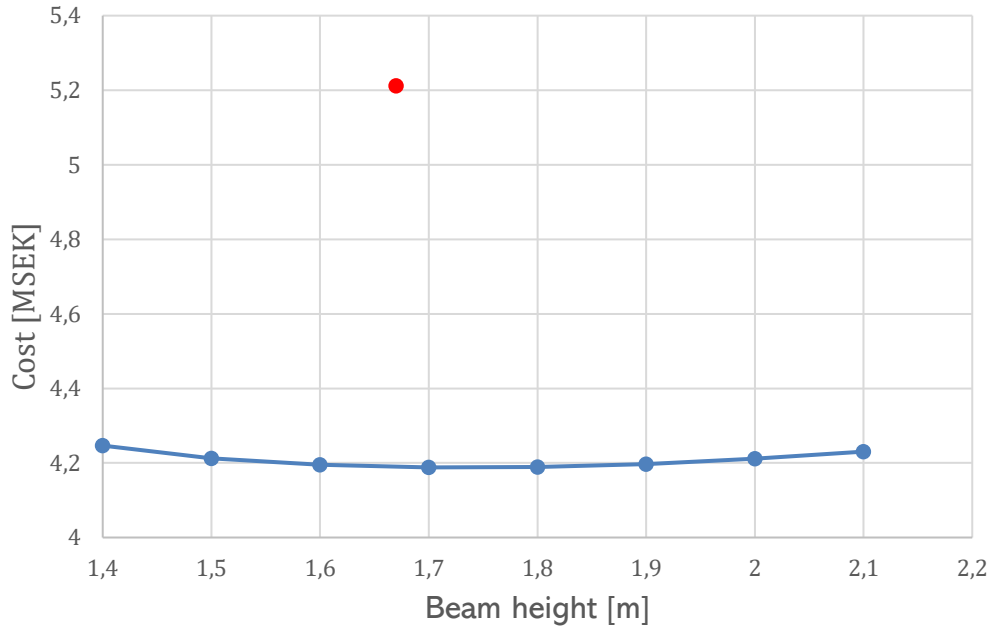

Figure 6.6 *Cost of the existing bridge compared to optimized bridge soultions with different beam heights.*

Figure 6.7 shows the GWP of the existing and the optimized bridge solutions in Figure 6.5.

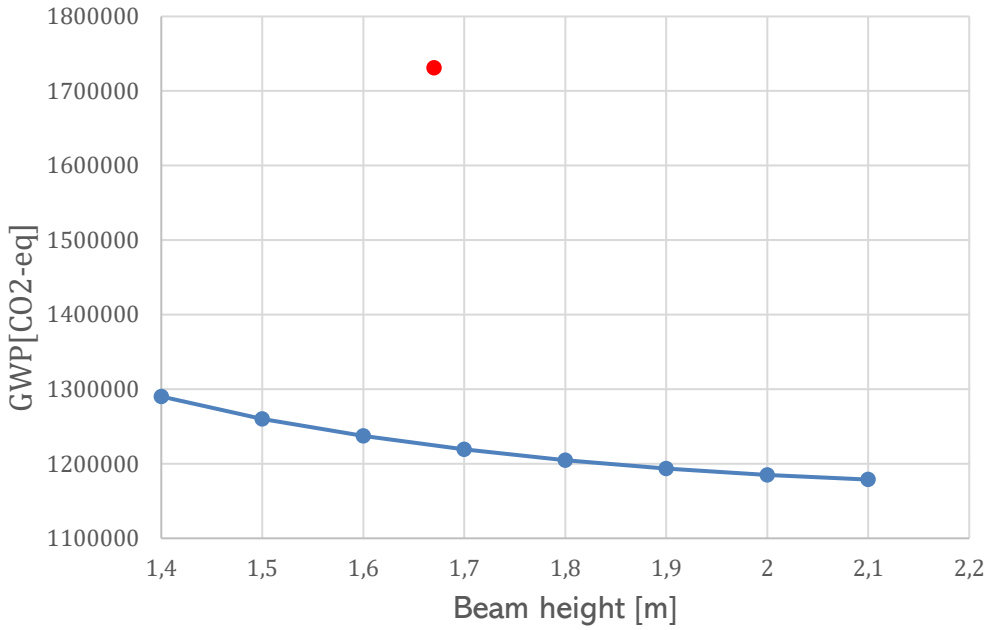

Figure 6.7 *GWP of the existing bridge compared to optimized bridge soultions with different beam heights.*

Table 6.5 *Reduction of cost and GWP for the optimized bridge solutions in comparison with the existing bridge 100-411-1.*

Bridge name	**100-411-1**
Reduction of cost	21%
Reduction of GWP	29%

6.4 Comparison between optimized and existing bridge including reinforcement splicing

The optimization process provides the amount of non-prestressed reinforcement needed without accounting for the anchorage of reinforcement. Therefore, the actual amount of non-prestressed reinforcement should be increased to include the splicing lengths where the reinforcement bars are spliced to each other by overlapping. Splicing lengths adds to the amount of non-prestressed reinforcement and the difference between the existing bridge and the optimized bridge solutions decreases. Figure 6.8 presents the amount of reinforcement for the existing bridge and for different beam heights for the optimized bridge including lapping.

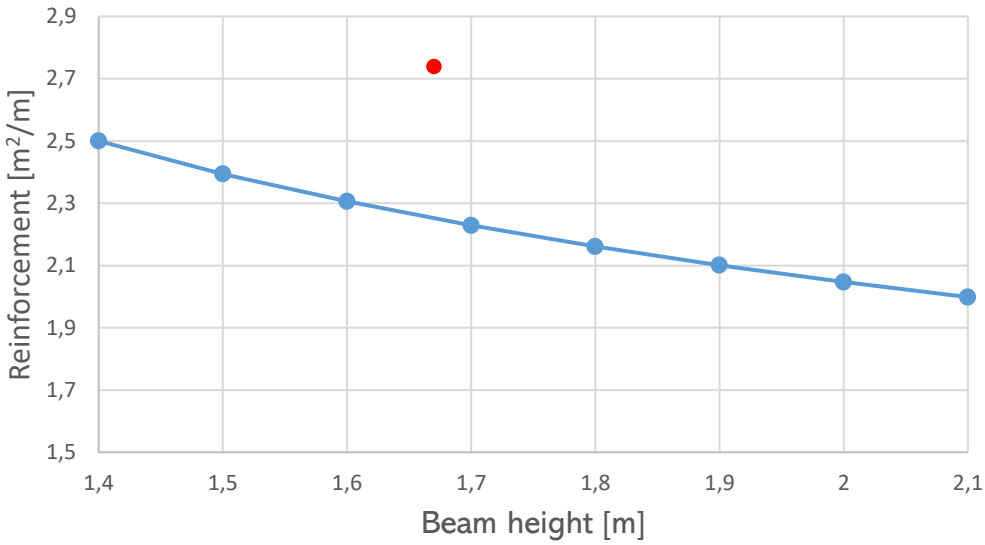

Figure 6.8 *Comparision of non-prestressed reinforcement quantities between the existing bridge and corresponding optimized bridge solutions, including reinforcement splicing.*

Figure 6.9 shows the total cost of the existing and the optimized bridge solutions, including reinforcement splicing, in Figure 6.8.

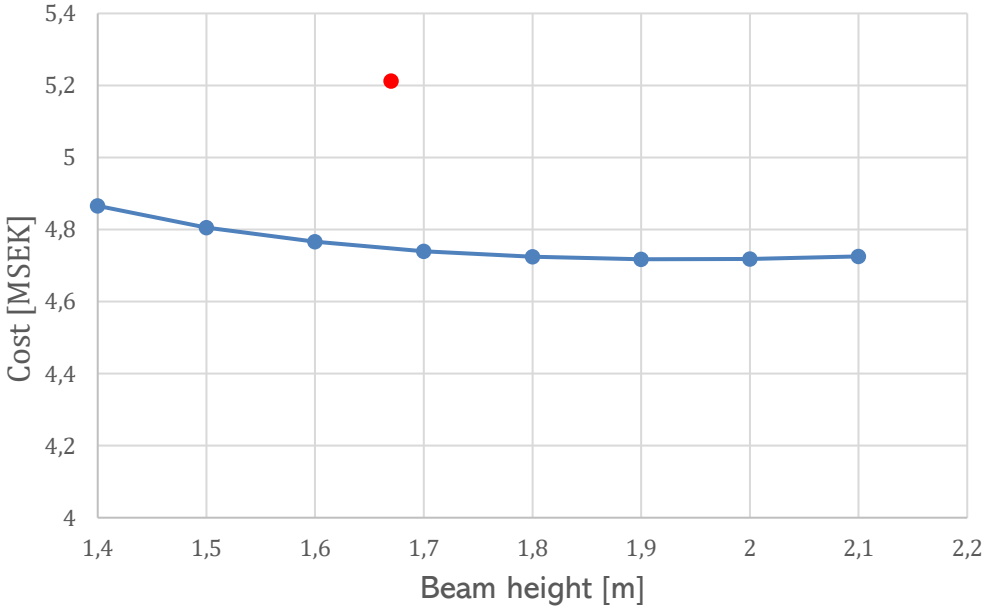

Figure 6.9 *Cost of the existing bridge compared to optimized bridge soultions with different beam heights, including reinforcement splicing.*

Figure 6.10 shows the GWP of the existing and the optimized bridge solutions, including reinforcement splicing, in Figure 6.8.

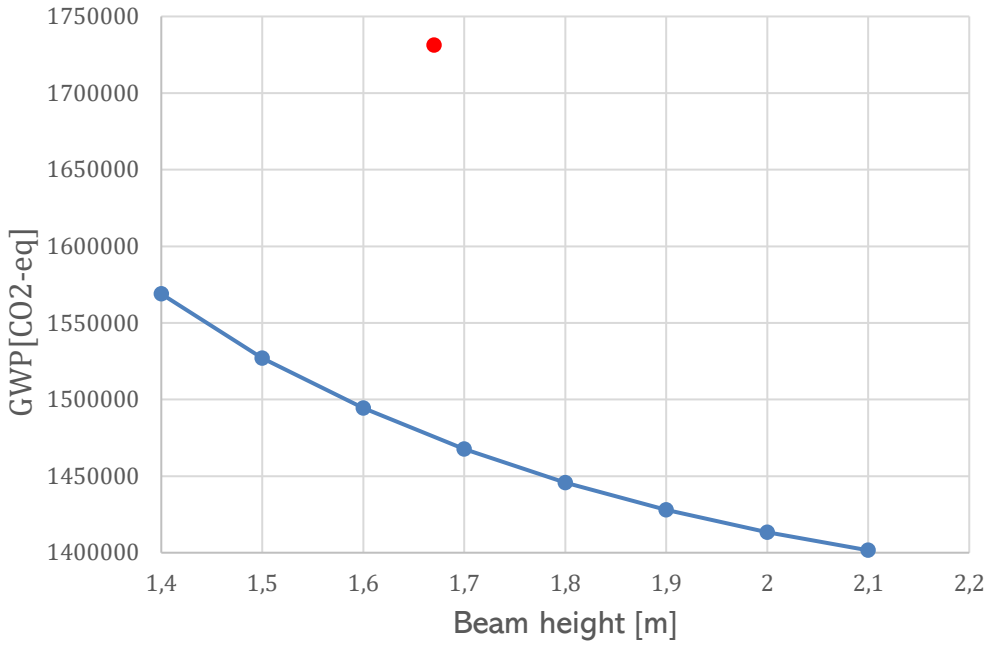

Figure 6.10 *GWP of the existing bridge compared to optimized bridge soultions with different beam heights, including reinforcement splicing.*

Table 6.6 *Reduction of cost and GWP for optimized bridge solutions, including reinforcement splicing, in comparison with the existing bridge 100-411-1.*

Bridge name	**100-411-1**
Reduction of cost	9.6%
Reduction of GWP	15.2%

7 Discussion

In this chapter, the results are discussed. The discussion is divided into two parts: Section 7.1 focuses on the relations between beam height, amount of non-prestressed reinforcement and cracking angle, and the performance with regard to cost and GWP. Section 7.2 is a comparison between optimized bridge solutions and an existing bridge.

7.1 General Results

The results in Section 6.1 show that higher beams give smaller quantities of non-prestressed reinforcement, for both bridges studied. Since increasing the height of the concrete cross-section gives more capacity against shear and torsion, the required non-prestressed reinforcement in the beam decreases. This leads to a lower GWP because the reduced amount of reinforcement has a higher impact on greenhouse gas emissions in comparison with the increased amount of concrete. However, the influence of increased height is not so clear from an economic point of view, as Figure 6.2 shows. In bridge 1, the somewhat shorter and narrower bridge, the beam height 2.1 m gives the lowest cost, because this height gives the minimum amount of non-prestressed reinforcement. In bridge 2, the beam height 1.8 m gives the lowest cost and here it depends on how much the amount of reinforcement increases in relation to increase of beam height

In section 6.2, the span lengths of bridges 1 and 2 are varied. It is noticeable that longer spans require more non-prestressed reinforcement per meter span length in comparison with shorter spans when beam height, inclination of compressive struts and number of tendons are the same. For example, Table 6.5 shows that bridge 1 with the span length 32 m has more non-prestressed reinforcement than the span 30 m, where the beam height, inclination of compressive struts and number of tendons are the same. This is also true for the spans 28 m and 30 m in bridge 2. However, when any of these parameters are changed, reinforcement quantities change as well.

The inclination of compressive struts, θ, influences the amount of non-prestressed reinforcement per meter span length in the bridge. The chosen step size in the set of the angles is small in order to get accurate quantities for the reinforcement. A smaller inclination of compressive struts leads to less shear reinforcement and more longitudinal reinforcement because of the increase of stresses in the tensile chord. If the longitudinal reinforcement is decisive and has the most significant effect on quantities of reinforcement in the bridge, a steeper angle will give less non-prestressed reinforcement. This can be seen for the longer span 36 m of bridge 1, which has less reinforcement and a larger inclination angle than the shorter span length 34 m, seeTable 6.5. The general pattern is that longer spans need more longitudinal reinforcement due to the increase of the shear force and torsional moment.

It should be noted that the results with respect to economic optimization depends on the current material prices. Recently, the price of the steel had increased about 44% (Statiska centralbyrån, 2022) in comparison with the previous year. Consequently, the prices in this thesis do not represent the actual current prices since the input data is based on Aspegren & Möörk (2021).

7.2 Comparison with existing bridge 100-411-1

The comparison between the existing bridge 100-411-1 and the optimized bridge solutions shows that the beam heights and non-prestressed reinforcement amounts could be decreased compared to what was used in engineering practice. All obtained optimized solutions give a lower cost and GWP than the existing bridge.

As described in section 6.4, splicing is not included in the optimization method. Consequently, the reinforcement amounts increase when the double reinforcement bars along the overlapping splices is taken into account. The increase of non-prestressed reinforcement quantities due to splicing was calculated to 27% of the original quantities. This is reasonable according to experienced structural engineers since additional reinforcement due to splicing usually is 25% to 30%. Also, when splicing is taken into account, all obtained optimized solutions show lower cost and GWP than the existing bridge. Table 6.7 shows that the optimized bridge has a decreased cost of approximately 10% in comparison with the existing bridge. The influence on GWP is larger and the optimized bridge has approximately 15% smaller GWP in comparison with the existing bridge.

8 Conclusion

An existing tool developed by Aspegren & Möörk (2021) for optimization of two-span continuous prestressed concrete beam bridges, has been further developed in this master thesis. The optimization tool resulted in bridges with more material efficient solutions in comparison with existing bridge designs. In a case study the cost and GWP were reduced by approximately 10 % and 15%, respectively, in comparison with a recently constructed bridge, bridge 100-411-1. The results show that a higher beam height gives the less reinforcement. Moreover, the results show that for both slim and wide bridges, GWP is decreased for higher beams. With the material costs used in the study, the beam height has no major impact on the cost of the bridges. However, it is likely that a higher beam height will result in lower costs with the recently sharply increased steel prices .

The optimization method used by Aspegren & Möörk (2021) is based on an iterative process to obtain the lowest cost and GWP, and determines the cable geometry, beam height and number of cables that are optimal according to both cost and GWP. The geometry and number of cables were not varied in this study in order to focus on the non-prestressed reinforcement. The optimal amount of non-prestressed reinforcement is thereafter obtained by changing the inclination of compressive strut and beam height that fulfill the design checks. Smaller angles give a smaller amount of stirrups reinforcement but a higher amount of longitudinal reinforcement. Since the assumptions of the work done by Aspegren & Möörk (2021), such as web to flange width ratio, resulted in savings in terms of both GWP and cost, the same assumptions were made in this thesis.

The bridge designs obtained by the optimization method were better with respect to both cost and GWP compared to the experience-based bridge designs. Therefore, this method can be implemented to obtain more optimal design solutions in early design stages. Implementing set-based parametric design (SBPD) method is beneficial for bridge design in preliminary design phase, since the most optimal solutions are dependent on the combination of different parameters. Finally, the optimization method shows a potential in generating better design solutions that are both environmentally and economically profitable. As the result shows, a higher beam height may be considered as a better solution in contrary of the conclusions drawn in the previous thesis by Aspegren & Möörk (2021), where the non-prestressed reinforcement was not included in the optimization.

8.1 Further studies

The analysis has been developed to include the non-prestressed reinforcement in this thesis. It was shown that it is important to include also the non-prestressed, and not only the prestressing reinforcement already in the early design phase to make optimal design choises. However, simplifications was still made regarding the bridge layout. Consequently, more studies can be performed on the tool to include additional parts of bridge design to get more accurate results.

The check of cracking could be included more accurately in the design tool by comparing the calculated tensile stress with the lower characteristic tensile strength, which would decrease the required prestressed force. This could lead to a more accurate optimization with respect to both economy and GWP due to that a smaller required prestressed force would result in a smaller number of strands to fulfil the crack check.

The values of the inclination of compressive struts and the geometries of the bridges had an influence on the optimization. However, in the current study, their variation was not included in detail. Therefore, additional investigation could be performed in order to develop and implement a more detailed optimization with respect to compressive strut angles and dimensions of the bridges. This can be obtained in two different ways. Additional values of inclination of compressive struts could be easily added in the optimization tool. However, the most optimal solution depends also on the geometry of the bridges. Therefore, an additional investigation of the design of wing walls, end screen walls and the cross beam could lead to a more accurate width of cross section for the bridge beams, which would likely result to an even more optimized bridge design.

In this thesis the optimization tools have obtained beneficial results and it can be used for other bridges type in an advanced process design, since the non-prestressed reinforcement is included in the tool as well.

9 References

Aspegren, D. & Möörk, E. (2021). *Early estimations of dimensions for prestressed concrete bridges*. Master Thesis. Department of Architecture and Civil Engineering, Chalmers University of Technology, Gothernburg, Sweden, 62 pp. Available at: https://hdl.handle.net/20.500.12380/304088 (Retrieved 2022-01-21)

Alhede, A. & Beskow, K. (2021). *Parameter Study and Optimization of Slab Frame Bridges.* Master Thesis. Department of Architecture and Civil Engineering, Chalmers University of Technology, Gothernburg, Sweden, 62 pp. Available at: https://odr.chalmers.se/handle/20.500. 12380/301443 (Retrieved 2022-01-21)

Bhatt, P. (2011). *Prestressed concrete design to eurocodes*. CRC Press, London, 616 pp. Available at: https://doi.org/10.1201/b12839 (Retrieved 2022-02-02)

Boverket. (2021). *Utsläpp av växthusgaser från bygg- och fastighetssektorn.* (Emissions of greenhouse gases from the construction and real estate sector. In Swedish). Available at: https://www.boverket.se/Sv/Byggande/Hallbart-Byggande-Och-Forvaltning/Miljoindikatorer---Aktuell-Status/Vaxthusgaser/ (Retrieved 2022-01-26)

Energimyndigheten. (2021). *Industrin – nuläge och förutsättningar för omställning.* Available at: Energimyndighetens webbshop (a-w2m.se) (Retrieved 2022-02-03)

Engström, B. (2011). *Design and analysis of prestressed concrete structures.* Chalmers University of Technology, Gothernburg, Sweden, 192 pp. Available at: https://www.chalmersstore.se/kompender/design-and-analysis-of-prestressed-concrete-structures.html (Retrieved 2022-02-05)

Engström, B. (2015). *Design and analysis of continuous beams and columns.* Chalmers University of Technology, Gothernburg, Sweden, 133 pp. Available at: https://www.chalmersstore.se/kompender/design-and-analysis-of-prestressed-concrete-structures.html (Retrieved 2022-02-05)

Fu, f. (2018). *Design and Analysis of Tall and Complex Structures*. Butterworth-Heinemann, ISBN 978-0-08-101018-1, Oxford, United Kingdom, 2018, 293 pp. Available at https://ebookcentral.proquest.com/lib/chalmers/detail.action?docID=5257306 (Retrieved 2022-02-010)

Gao, Q. Liu, B. Sun, J. Liu, C. Youquan, X. (2021). *Trade decomposition of CO2 emissions of global construction industries.* Available at: (PDF) Trade decomposition of CO 2 emissions of global construction industries (researchgate.net) (Retrieved 2022-02-21)

Girardet, A. & Boton, C. (2021). A parametric BIM approach to foster bridge project design and analysis. *Automation in Construction,*Vol. 126, March 2021, 23 pp . Available at: https://www.sciencedirect.com/science/article/pii/S0926580521001308 (Retrieved 2022-02-12)

Gosavi, A. *Simulation-based optimization: parametric optimization techniques and reinforcementlearning*. Springer, ISBN978-1-4899-7490-7, NewYork, US, 2015, 504 pp. Available at: https://link.springer.com/book/10.1007/978-1-4899-7491-4 (Retrieved 2022-02-12)

Rempling, R. Mathern, A. Ramos, D. Fernández, S. (2019). Automatic structural design by a set-based parametric design method. *Automation in Construction,* Vol 108, 10 pp. Available at: https://www.sciencedirect.com/science/article/pii/S0926580518303042 (Retrieved 2022-02-07)

Ruijven, B. (2016). Long-term model-based projections of energy use and CO2 emission from the global steel and cement indusries. *Resources, Conservation and Recycling*, Vol. 181, 25 pp. 15-36. Available at: https://www.sciencedirect.com/science/article/pii/S0921344916301008?via%3Dihub (Retrieved 2022-02-21)

Scanscot Technology. (2021). *BRIGADE/Plus 6.2-20*

SIS. (2002a). *Eurokod - Grundläggande dimensioneringsregler för bärverk*

SIS. (2002b). *Eurokod 1: Laster på bärverk - Del 1-1: Allmänna laster – Tunghet, egentyngd, nyttig last för byggnader. 08(121687).*

SIS. (2003a). *Eurokod 1 : Laster på bärverk – Del 2 : Trafiklast på broar. Svenska institutet för standarder. Stockholm.*

SIS. (2003b). *Eurokod 1 : Laster på bärverk – Del 1-5 :Allmänna laster - Temperaturenpåverkan*

SIS. (2005a). *Eurokod 2: Dimensionering av betongkonstruktioner -Del 1-1:Allmänna regler och regler för byggnader. In Euro code SS-EN-1191-2 (Issue 138227)*

SIS. (2005b). *Eurokod 2: Dimensionering av betongkonstruktioner - Del 2: Broar. In Eurokod SS-EN-1191-2*

Statistiska centralbyrån. (2022). *Construction costs rose by 0.9 percent in february. Retrieved May 26, 2022,* from *https://www.scb.se/en/finding- statistics/ statistics - by - subject - area/prices - and - consumption/building - price -index - and-construction-cost-index-for-bu/construction-cost-index-for-buildingscci-input-price-index/pong/statistical- news/construction- cost-index-forbuildings-february-2022/*

Trafikverket. (2019a). *Krav Brobyggande TDOK 2016:0204.* Available at: *https://trvdokument.trafikverket.se/Versioner.aspx?spid=4052&dokumentId=TDOK%202016%3A0204* (Retrieved 2022-02-02)

Trafikverket. (2019b). *Bärighetsberäkning av broa TDOK 2013:0267.* Available at: *https://trvdokument.trafikverket.se/Versioner.aspx?spid=5403&dokumentId=TDOK%202013%3A0267* (Retrieved 2022-02-07)

Transportstyrelsen. (2018). *Transportstyrelsens föreskrifter och allmänna råd om tillämpning av eurokoder TSFS 2018:57 https://www.transportstyrelsen.se/TSFS/TSFS%202018_57.pdf* (Retrieved 2022-02-03)